Title: Gut microbiome compositional and functional features associate with Alzheimer's disease pathology

Authors:

Jea Woo Kang[1]*, Lora A. Khatib[2,3]*, Margo B. Heston[1]*, Amanda H. Dilmore[2], Jennifer S. Labus[4,5,6], Yuetiva Deming[1], Leyla Schimmel[7], Colette Blach[8], Daniel McDonald[2], Antonio Gonzalez[2], MacKenzie Bryant[2], Karenina Sanders[2], □ara Schwartz[2], Tyler K. Ulland[1,9], Sterling C. Johnson[1], Sanjay Asthana[1], Cynthia M. Carlsson[1], Nathaniel A. Chin[1], Kaj Blennow[10], Henrik Zetterberg[10,11,12,13,14,1], Federico E. Rey[15], Alzheimer Gut Microbiome Project Consortium[7], Rima Kaddurah-Daouk[7,16,17], Rob Knight[2,18,19,20,21], and Barbara B. Bendlin[1,22,#]

*These three authors contributed equally to this work.
[#]Correspondence

Affiliations and addresses:

1. Wisconsin Alzheimer's Disease Research Center, University of Wisconsin School of Medicine and Public Health, University of Wisconsin-Madison, Madison, WI, USA
Address: 600 Highland Ave, J5/1 Mezzanine, Madison, WI, USA 53792
2. Department of Pediatrics, University of California San Diego, La Jolla, California, USA
Address: 9461 Gilman Dr, La Jolla, CA, USA 92093
3. Neurosciences Graduate Program, University of California San Diego, La Jolla, California, USA
Address: 9500 Gilman Dr, La Jolla, CA, USA 92093
4. Integrative Biostatistics and Bioinformatics Core (IBBC) at the Goodman-Luskin Microbiome Center
Address: 42-210 CHS, Los Angeles, CA, USA 90095
5. G. Oppenheimer Center for Neurobiology of Stress and Resilience
Address: 10833 Le Conte Ave, Los Angeles, CA, USA 90095
6. UCLA Vatche and Tamar Manoukian Division of Digestive Diseases, David Geffen School of Medicine at UCLA
Address: 100 Medical Plaza, Los Angeles, CA, USA 90095
7. Department of Psychiatry and Behavioral Sciences, Duke University, Durham, NC, USA
Address: 905 W Main St, Durham, NC, USA 27701
8. Duke Molecular Physiology Institute, Duke University, Durham, NC, USA
Address: 300 N Duke St, Durham, NC, USA 27701
9. Department of Pathology and Laboratory Medicine, University of Wisconsin-Madison, Madison, WI, USA
Address: 1685 Highland Ave, Madison, WI, USA 53705
10. Department of Psychiatry and Neurochemistry, Institute of Neuroscience and Physiology, the Sahlgrenska Academy at the University of Gothenburg, Mölndal, Sweden

Address: Blå stråket 15, vån 3 SU/Sahlgrenska 413 45 Göteborg, Sweden

11. Clinical Neurochemistry Laboratory, Sahlgrenska University Hospital, Mölndal, Sweden
Address: Blå stråket 5, 413 45 Göteborg, Sweden

12. Department of Neurodegenerative Disease, UCL Institute of Neurology, Queen Square, London, UK
Address: Queen Square, London WC1N 3BG, United Kingdom

13. UK Dementia Research Institute at UCL, London, UK
Address: 6th Floor, Maple House, Tottenham Ct Rd, London W1T 7NF, United Kingdom

14. Hong Kong Center for Neurodegenerative Diseases, Clear Water Bay, Hong Kong, China
Address: Units 1501-1502, 1512-1518, 15/F, Building 17W, Hong Kong Science Park, Shatin, N.T., Hong Kong

15. Department of Bacteriology, University of Wisconsin-Madison, Madison, WI, USA
Address: 1550 Linden Dr, Madison, WI, USA 53706

16. Duke Institute of Brain Sciences, Duke University, Durham, NC, USA
Address: 308 Research Dr, Durham, NC, USA 27710

17. Department of Medicine, Duke University, Durham, NC, USA
Address: 40 Duke Medicine Circle, 124 Davison Building, Durham, NC, USA 27710

18. Center for Microbiome Innovation, Joan and Irwin Jacobs School of Engineering, University of California San Diego, La Jolla, California, USA
Address: Franklin Antonio Hall, Jacobs School of Engineering, 9500 Gilman Dr, La Jolla, CA, USA 92093

19. Department of Computer Science and Engineering, University of California, San Diego, La Jolla, CA, USA
Address: 3235 Voigt Dr, La Jolla, CA, USA 92093

20. Halıcıoğlu Data Science Institute, University of California, San Diego, La Jolla, CA, USA
Address: 3234 Matthews Ln, La Jolla, CA, USA 92093

21. Shu Chien-Gene Lay Department of Bioengineering, University of California, San Diego, La Jolla, CA, USA
Address: 3223 Voigt Dr, La Jolla, CA, USA 92093

22. Wisconsin Alzheimer's Institute, School of Medicine and Public Health, University of Wisconsin-Madison, Madison, WI, USA
Address: 610 Walnut Street, 9th Floor, Madison, WI, USA 53726

Abstract

BACKGROUND: The gut microbiome is a potentially modifiable factor in Alzheimer's disease (AD); however, understanding of its composition and function regarding AD pathology is limited.

METHODS: Shallow-shotgun metagenomic data was used to analyze fecal microbiome from participants enrolled in the Wisconsin Microbiome in Alzheimer's Risk Study, leveraging clinical data and cerebrospinal fluid (CSF) biomarkers. Differential abundance and ordinary least squares regression analyses were performed to find differentially abundant gut microbiome features and their associations with CSF biomarkers of AD and related pathologies.

RESULTS: Gut microbiome composition and function differed between people with AD and cognitively unimpaired individuals. The compositional difference was replicated in an independent cohort. Differentially abundant gut microbiome features were associated with CSF biomarkers of AD and related pathologies.

DISCUSSION: These findings enhance our understanding of alterations in gut microbial composition and function in AD, and suggest that gut microbes and their pathways are linked to AD pathology.

1 BACKGROUND

The human gut microbiome is recognized as an important modifiable factor in health and disease. It is related to overall gut health by maintaining gut barrier integrity and gut immune homeostasis via balanced composition and production of microbial metabolites such as short-chain fatty acids (SCFAs).[1–3] However, in certain disease states, including Alzheimer's disease (AD), gut microbiome composition and its metabolic changes may alter and exacerbate the disease.

Compositional differences in gut microbiota, including relative abundance and diversity, have been observed between control and AD groups.[4] Other studies have reported that gut microbiome composition is altered among people with AD dementia, individuals with mild cognitive impairment (MCI), or preclinical AD compared with healthy controls.[5–8] To better determine the relationship between gut microbiome and AD pathology, studies have leveraged measures of AD biomarkers obtained via cerebrospinal fluid (CSF) analysis,[9] positron emission tomography (PET),[10] and plasma.[11] Additionally, inflammatory markers have been utilized to find associations with gut inflammation-driven AD pathology.[12,13]

The shift towards functional analysis provides deeper insights into the functional potential of the microbiome, which is important given that multiple lines of evidence indicate that gut microbial pathways and associated metabolites influence disease development, as well as providing the opportunity to identify therapeutic targets.[14–17] A small number of studies have examined gut microbiome composition and function together with markers of AD pathology in humans,[8,18–20] but many other studies to date are limited to the composition of gut microbes in a single cohort. The Alzheimer Gut Microbiome Project (AGMP) initiative continues to leverage gut microbiome and metabolome to better understand metabolic processes that influence AD pathology.

To identify differences in composition and function as well as relationships between gut microbiome and AD pathology, this study collected stool samples from participants enrolled in the Microbiome in Alzheimer's Risk Study (MARS). Differences in microbiome diversity as well as abundance were compared between AD-related groups (diagnosis, amyloid status, and *APOE ε4* status), and the co-occurrence of the common gut microbiota features was analyzed among comparison groups. In addition, validation of gut microbiota composition that was differentially abundant between AD compared to healthy controls was performed in a larger cohort of participants who are part of the AGMP. Furthermore, determination of microbiome functional differences was compared between people with AD dementia and cognitively unimpaired (CU) individuals. Lastly, associations between any differentially abundant gut microbiome features were examined in relation to CSF biomarkers of AD and related pathologies to identify the potential microbes and microbial pathways that relate to AD pathology. We hypothesized that gut microbiome alterations in composition and function would be present among people with AD dementia compared to CU, as well as associate with AD pathology.

2 METHODS

2.1 Participants

Participants included in this study were recruited from the Wisconsin Alzheimer's Disease Research Center (ADRC) Clinical Core and the Wisconsin Registry for Alzheimer's Prevention (WRAP).[21] The WRAP study enrolled participants between the ages of 40–65 years at study entry, and the cohort is enriched for parental history of AD dementia. The Wisconsin ADRC clinical core enrolls participants who span the clinical and biological spectrum of AD, from those who are CU to individuals with mild cognitive impairment (MCI) and AD dementia. Participants underwent *APOE* genotyping using competitive allele-specific PCR-based KASP™ genotyping assays (LGC Genomics, Beverly, MA)[22] as well as longitudinal assessments of cognition and laboratory tests. Biomarkers of AD determined with CSF collection and PET neuroimaging were collected in a subset of the cohort. Participants underwent fecal sample collection as part of their participation in MARS, which was used to analyze the gut microbiome. Participants completed questionnaires including medical history and diet, at the time of fecal sample collection.

Participant diagnosis of AD was determined by a multidisciplinary consensus diagnostic panel and based on the National Institute on Aging–Alzheimer's Association (NIA-AA) criteria.[23,24] Participants underwent dynamic [C-11]Pittsburgh compound B (PiB) PET scans and lumbar puncture for CSF collection to determine their amyloid status. Amyloid positivity on PET imaging was achieved by the visual rating (1.19 or greater)[25] from a global PiB distribution volume ratio (DVR) and determined for CSF via the $A\beta_{42}/A\beta_{40}$ ratio (less than 0.046).[26] The study procedures were approved by the University of Wisconsin Institutional Review Board, and all participants provided signed or oral informed consent.

An independent cohort of participants who are part of the AGMP and who were recruited from multiple NIA-funded ADRC across the U.S. (n = 448, **Table S1**) was included for validation of differential abundance analysis. AGMP participants from Wisconsin were excluded to ensure a unique validation sample.

2.2 Fecal sample collection and metagenomic data sequencing

Fecal samples were collected as previously described.[4] Briefly, participants collected their stool samples at home with provided fecal collection kits. Participants returned their samples in insulated containers which were chilled with frozen gel packs. Returned samples were immediately weighed and scored on the Bristol stool scale. Fecal samples were then subsampled using sterile straws and stored at −80°C until processing.

Fecal samples were processed for DNA extraction as previously described.[27] Briefly, samples were extracted using the MoBio PowerMag Soil DNA isolation kit with a magnetic bead plate. Extracted genomic DNA (gDNA) was quantified with Quant-iT PicoGreen double-stranded DNA (dsDNA) assay kit (Thermo Fisher Scientific Inc.), and underwent a miniaturized KAPA HyperPlus library preparation using an iTru indexing strategy.[28,29] Library was normalized pooled based on concentration, PCR cleaned, and then size selected (300-700 bp) on the Sage Science PippinHT. Libraries were sequenced on an Illumina NovaSeq 6000 as a paired-end

150-cycle run at the University of California San Diego (UCSD) IGM Genomics Center as part of AGMP initiative.[30]

2.3 Metagenomic data processing

The metagenomic data processing was performed as previously described.[31] The sequence data were filtered for all adapters known to fastp (version 0.23.4) in paired-end mode by explicitly specifying a known adapters file.[32] Fastp also removed sequences shorter than 45 nucleotides with -l, a flag to filter the minimum length of each sequence. Each sample was then filtered against each genome in the human pangenome,[33] as well as both T2T-CHM13v2.0[34] and GRCh38,[35] using minimap2[36] (version 2.26-r1175) with "-ax sr" for short read mode. The data were first run in paired-end mode, and then run in single-end mode, per genome. Each successive run was converted from SAM to FASTQ using samtools[37] (version 1.17) with arguments -f 12 -F 256 -N for paired-end data and -f 4 -F 256 for single-end. The single-end data are repaired using fastq_pair[38] (version 1.0) specifying a table size of 50M with -t. Compute support was provided with GNU Parallel[39] (version 20180222). Single-end FASTQ output from samtools was split into R1 and R2 with a custom Rust program, with rust-bio for parsing[40] (version 1.4.0). Data were multiplexed with sed and demultiplexed using a custom Python script. Shotgun sequencing data were then uploaded to and processed through Qiita[41] (Study ID 13663). Sequence adapter and host filtering were executed using qp-fastp-minimap2 version 2022.04. Subsequently, Woltka[42] version 0.1.4 (qp-woltka 2022.09) with the Web of Life 2 database was employed for taxonomic and functional predictions. Genomic coverages were computed, and features with less than 25% coverage were excluded.[43] To enhance data quality, a prevalence filter using QIIME 2 v2023.5[44] was applied, eliminating features present in less than 10% of samples and samples with a sampling depth of less than 500,000 reads to mitigate the inclusion of erroneous and low-quality reads. The resulting feature table was utilized for downstream analysis.

2.4 Biomarker measurements

2.4.1 CSF biomarkers

CSF samples were collected via lumbar puncture in the morning after fasting for 8-12 hours as previously described.[26] CSF biomarkers were measured using the NeuroToolKit (NTK), a panel of exploratory robust prototype assays (Roche Diagnostics International Ltd, Rotkreuz, Switzerland). The following biomarkers were quantified on the Cobas® e 601 module (Roche Diagnostics International Ltd, Rotkreuz, Switzerland): $A\beta_{42}$, $pTau_{181}$, tTau, S100 calcium binding protein B (S100B), and interleukin-6 (IL-6), and the remaining biomarkers were assayed on the Cobas® e 411 analyzer: $A\beta_{40}$, neurofilament light protein (NfL), neurogranin, α-synuclein, glial fibrillary acidic protein (GFAP), chitinase-3-like protein 1 (YKL-40), and soluble triggering receptor expressed on myeloid cells 2 (sTREM2). Each biomarker was measured as markers of AD and related pathologies which were amyloid pathology ($A\beta_{42}/A\beta_{40}$), tau pathophysiology ($pTau_{181}$ and tTau), neurodegeneration (NfL), synaptic dysfunction and injury (neurogranin and α-synuclein), inflammation (IL-6), and glial activation (S100B, GFAP, YKL-40, and sTREM2).

2.4.2 PiB PET biomarker

Dynamic ^{11}C-PiB scans were acquired using a Siemens ECAT EXACT HR+ tomograph as previously described.[45] DVRs were estimated with Logan graphical analysis and a threshold of 1.19 for global DVR was used to determine PiB status which was used along with CSF $A\beta_{42}/A\beta_{40}$ ratio to confirm amyloid status of participants.

2.5 Statistical analysis

Statistical analysis on participant demographics was performed across clinical diagnoses using the Kruskal-Wallis rank sum test for continuous variables and Pearson's Chi-squared test for categorical variables. Analysis with multiple comparisons was corrected for multiple tests employing the Bonferroni correction method. Gut microbiome diversities were calculated using QIIME 2 tools.[44] Alpha diversity indices were calculated including Shannon,[46] Evenness,[47] and Faith's phylogenetic diversity (PD).[48] Beta diversity indices were calculated including Bray–Curtis dissimilarity,[49] and Weighted[50] and Unweighted[51] UniFrac. The Bayesian Inferential Regression for Differential Microbiome Analysis (BIRDMAn) pipeline was used for microbiome differential abundance (DA) analysis.[52] Microbiome features (composition and function) were outcome variables and each AD-related group (clinical diagnosis, amyloid status, and *APOE ε4* status) was a predictor adjusting for covariates including age, sex, BMI, Bristol type, medication status, and age difference between fecal collection and measurements of each predictor variable. Log ratios of Top and Bottom features of each AD-related group (log[Top features/Bottom features]) were calculated and analyzed using the Mann–Whitney *U* test to identify similarities in microbiome features that differ between AD-related groups. Venn diagrams were created to illustrate any overlapping taxonomies across AD groups in each Top (more abundant in AD-related groups) and Bottom (less abundant in AD-related groups) group at each taxonomic level (phylum, family, genus, and species). Log ratios of Top and Bottom features of each AD group (log[Top features/Bottom features]) were also calculated and analyzed using the Mann–Whitney *U* test in MARS and validation cohorts to identify similarities in microbiome features that differ between AD and CU groups in both cohorts. Log ratios of Top and Bottom functional features (log[Top features/Bottom features]) were calculated and statistical significance was determined by the Mann–Whitney *U* test between AD and CU groups. Differentially abundant KEGG Orthology (KO)[53] pathways and their associated species were determined using BIRDMAn.[52] Robust Aitchison principal component analysis (RPCA) from Gemelli (version 0.0.10) was used to analyze sparse compositional KO[53] microbiome pathway features that are separated by sample variations.[54] RPCA results were visualized with scores plots and biplots. Statistical analysis on RPCA was performed with permutational multivariate analysis of variance (PERMANOVA)[55] between groups.

To explore the relationships between key microbial features and pathways identified via BIRDMAn and CSF biomarkers of AD and related pathologies, we applied an ordinary least squares (OLS) linear regression approach. Prior to fitting the linear regression model, CSF biomarkers were standardized using the StandardScaler (version 0.24.1) from the scikit-learn library.[56] To address issues with sparse, compositional data, we used the multiplicative_replacement function from the scikit-bio (version 0.5.7) skbio.stats.composition module to preprocess the metagenomics data. This function replaces zeros with small positive

values, preserving the compositional nature of the data. Subsequently, a centered log ratio (CLR) transformation was applied to the metagenomics data to account for compositionality. Finally, ordinary least squares (OLS) linear regression was performed on the microbial features differentially abundant in AD versus CU, in relation to each CSF biomarker. The results were visualized using heatmaps.

All other statistical analyses were performed using Python libraries SciPy (1.13.0),[57] scikit-learn (1.4.2),[56] and NumPy (version 1.26.4).[58] All figures were generated using Python libraries Matplotlib (version 3.6.0)[59] and Seaborn (version 0.11.2).[60]

3 RESULTS

3.1 Participant demographics

Participant characteristics are shown by clinical diagnosis in **Table 1**. Participants were aged between 47-93 years. The mean age differed significantly in dementia-AD vs CU. The percent ratio of *APOE ε3/ε3* carriers was significantly lower and the percent ratio of *APOE ε4/ε4* carriers was higher in dementia-AD compared to CU. Amyloid positivity was higher in the AD dementia group.

3.2 Diversity results in gut microbiota composition

Alpha diversity indices (Shannon, Evenness, and Faith's PD) were presented on the y-axis and all AD group categories were presented on the x-axis (**Figure 1A-I**). The only comparison with significant alpha diversity differences was the *APOE ε4* comparison (**Figure 1G and H**). All alpha diversity indices showed significant differences or a trend toward differences between *APOE ε4+* and *APOE ε4−* groups. Individuals who were *APOE ε4−* had significantly higher alpha diversity than *APOE ε4+*.

Beta diversity indices (Bray–Curtis dissimilarity, and Weighted and Unweighted UniFrac) were visualized with principal coordinates analysis (PCoA) plots for each AD group (**Figure 1J-R**). Significant differences between groups based on clinical diagnosis (diagnosis) were observed with each metric (**Figure 1J-L**). Differences in beta diversity between amyloid-positive and amyloid-negative individuals were detected only with the Bray–Curtis dissimilarity index (**Figure 1M-O**). Individuals positive and negative for *APOE ε4* demonstrated differences with both the Bray-Curtis and Weighted UniFrac metrics, but not with Unweighted UniFrac (**Figure 1P-R**), suggesting that the relative abundance of major taxa rather than community membership is important in driving these differences.

3.3 Gut microbiota composition in clinical diagnosis, amyloid status, and *APOE ε4* status groups

A DA analysis on gut microbiota composition was performed based on clinical diagnosis, amyloid status, and *APOE ε4* status groups using BIRDMAn and visualized as forest plots (**Figure 2**). Gut microbiota taxonomic features that showed the most differences by the effect

size (log ratio) in each comparison group were displayed up to 20 features in each Top (more abundant) and Bottom (less abundant) group for taxonomic levels including phylum, family, genus, and species. DA analysis between AD and CU in clinical diagnosis showed distinct gut microbiota composition at each taxonomic level (**Figure 2A, D, G, and J**). At the phylum level, the abundance of phylum Firmicutes_A was lower in AD compared to CU (Bottom), and the abundance of phyla Bacteroidota, Patescibacteria, and Fusobacteriota was higher in AD compared to CU (Top) (**Figure 2A**). At the family level, families such as *Clostridiaceae*, *Turicibacteraceae*, *Pasteurellaceae*, *Dialisteraceae*, *Enterococcaceae*, and *Ruminococcaceae* were in the Bottom group and *Fusobacteriaceae*, *Nanogingivalaceae*, *Gemellaceae*, and *Bacteroidaceae* were in the Top group (**Figure 2D**). At the genus level, genera including *Clostridium_P*, *Ruminococcus*, and *Cryptobacteroides* were in the Bottom group and *Fusobacterium_A*, *Fusobacterium*, *Nanogingivalis*, and *Gemella* were in the Top group (**Figure 2G**). At the species level, species included in the Bottom group were *Cryptobacteroides* spp., *Clostridium_P perfringens*, *Turicibacter sanguinis*, *Prevotella hominis*, and *Prevotella copri*, and in the Top group were *Fusobacterium_A mortiferum*, *Fusobacterium nucleatum*, *Fusobacterium animalis*, *Nanogingivalis gingivitcus*, *Collinsella stercoris*, and *Collinsella tanakaei* (**Figure 2J**).

DA analysis between A+ and A− in amyloid status showed distinct gut microbiota composition at each taxonomic level (**Figure 2B, E, H, and K**). At the phylum level, the abundance of phylum Firmicutes_C was lower in A+ compared to A− (Bottom), and the abundance of phyla Thermoplasmatota and Campylobacterota was higher in A+ compared to A− (Top) (**Figure 2B**). At the family level, families such as *Neisseriaceae*, *Anaeroplasmataceae*, *Turicibacteraceae*, and *Ruminococcaceae* were in the Bottom group and *Nanogingivalaceae*, *Campylobacteraceae*, and *Coriobacteriaceae* were in the Top group (**Figure 2E**). At the genus level, genera including *Prevotella*, *Eubacterium_R*, and *Lactococcus* were in the Bottom group and *Fusobacterium*, *Nanogingivalis*, and *Acidaminococcus* were in the Top group (**Figure 2H**). At the species level, species included in the Bottom group were *Dialister hominis*, *Prevotella copri*, and *Prevotella hominis*, and in the Top group were *Nanogingivalis gingivitcus*, *Collinsella tanakaei*, and *Fusobacterium animalis* (**Figure 2K**).

DA analysis between *APOE ε4*+ and *APOE ε4*− in *APOE ε4* status analyses showed distinct gut microbiota composition at each taxonomic level (**Figure 2C, F, I, and L**). At the phylum level, the abundance of phyla Firmicutes_A, Firmicutes_C, Spirochaetota, and Synergistota was lower in *APOE ε4*+ compared to *APOE ε4*− (Bottom), and the abundance of phylum Bacteroidota was higher in *APOE ε4*+ compared to *APOE ε4*− (Top) (**Figure 2C**). At the family level, families such as *Selenomonadaceae*, *Neisseriaceae*, *Pasteurellaceae*, *Turicibacteraceae*, and *Clostridiaceae* were in the Bottom group and *Lactobacillaceae*, *Eubacteriaceae*, and *Bacteroidaceae* were in the Top group (**Figure 2F**). At the genus level, genera including *Ruminococcus* and *Clostridium_P* were in the Bottom group and *Enterobacter*, *Hafnia*, and *Lactobacillus* were in the Top group (**Figure 2I**). At the species level, species included in the Bottom group were *Prevotella hominis*, *Dialister* spp., and *Ruminococcus* spp., and in the Top group were *Enterobacter hormaechei_A*, *Hafnia proteus*, *Collinsella stercoris*, *Enterobacter cloacae*, and *Collinsella tanakaei* (**Figure 2L**).

Log ratios of microbiome counts were calculated between the sum of the Top and Bottom groups from DA analysis to test the overall significant differences of microbiome features between AD conditions (log[sum of Top features/sum of Bottom features]) (**Figure 3**).

Overall, there were significant differences in each AD-related group (diagnosis, amyloid, and *APOE ε4*) (**Figure 3A, E, and I**). Features that significantly differed between AD and CU also differed between *APOE ε4*+ and *APOE ε4*− (**Figure 3A and C**). Features that significantly differed between A+ and A− also differed between AD and CU (**Figure 3D and E**). Features that significantly differed between *APOE ε4*+ and *APOE ε4*− also differed between AD and CU (**Figure 3G and I**).

3.4 Common gut microbiota features in clinical diagnosis, amyloid status, and *APOE ε4* status groups

Venn diagrams were used to find common microbiome features across different AD conditions for each Bottom and Top group at each taxonomic rank (**Table S2**). At the phylum level, phyla Bacteroidota co-occurred between diagnosis and *APOE ε4* in the Top group (**Figure 4A**). Firmicutes_A co-occurred between diagnosis and *APOE ε4*, and Firmicutes_C co-occurred between amyloid and *APOE ε4* in the Bottom group (**Figure 4B**). In the Top group at the family level, the family *Lactobacillaceae* co-occurred across all conditions, families *Bacteroidaceae* and *Coprobacteraceae* between diagnosis and *APOE ε4*, and families *Nanogingivalaceae* and *Aerococcaceae* co-occurred between diagnosis and amyloid (**Figure 4C**). In the Bottom group, *UBA1829* and *Turicibacteraceae* co-occurred across all conditions (diagnosis, amyloid, and *APOE ε4*), families *CAG-508*, *CAG-74*, *Oscillospiraceae*, *Clostridiaceae*, *Pasteurellaceae*, and *CAG-138* co-occurred between diagnosis and *APOE ε4*, families *Ruminococcaceae*, *Anaeroplasmataceae*, and *CAG-312* co-occurred between diagnosis and amyloid, and family *Neisseriaceae* co-occurred between amyloid and *APOE ε4* (**Figure 4D**). Multiple genera and species co-occurred across all conditions (**Figure 4E-H**). In the Top group, the genus *Veillonella_A* co-occurred across all conditions, and the following numbers of genera co-occurred between each intersection, i.e., diagnosis and *APOE ε4*: 7, diagnosis and amyloid: 6, and amyloid and *APOE ε4*: 4 (**Figure 4E, Table S2**). In the Bottom group, 13 genera co-occurred across all conditions including *Prevotella* and *Turicibacter*, and the following numbers of genera co-occurred between each intersection, i.e., diagnosis and *APOE ε4*: 30, diagnosis and amyloid: 9, and amyloid and *APOE ε4*: 8 (**Figure 4F, Table S2**). In the Top group at the species level, 12 species including *Bacteroides ovatus*, *Collinsella tanakaei*, *Prevotella corporis*, and more co-occurred across all conditions, and the following numbers of species co-occurred between each intersection, i.e., diagnosis and *APOE ε4*: 18, diagnosis and amyloid: 10, and amyloid and *APOE ε4*: 7 (**Figure 4G, Table S2**). In the Bottom group, 27 species including *Ruminococcus_C callidus*, *Dialister succinatiphilus*, *Prevotella copri*, and more co-occurred across all conditions, and the following numbers of species co-occurred between each intersection, i.e., diagnosis and *APOE ε4*: 42, diagnosis and amyloid: 13, and amyloid and *APOE ε4*: 16 (**Figure 4H, Table S2**).

3.5 Validation of shallow-shotgun data with the ADRC dataset on gut microbiota composition

To validate the features linked with dementia-AD (AD) compared to healthy controls (CU), we tested the log-transformed ratios of features more and less abundant in AD in the MARS cohort against a larger cohort of participants who are part of the AGMP and who were recruited from multiple NIA-funded ADRC across the U.S. (n = 448; **Figure 5**). AGMP participants from Wisconsin were excluded to ensure a unique validation sample. The features that were differentially abundant in the MARS cohort (Kruskal-Wallis: 31.81, *P* value: < .001; **Figure 5A**) were also found to be differentially abundant in the larger validation cohort (Kruskal-Wallis: 5.59, *P* value: .02; **Figure 5B**).

3.6 Gut microbiome functional pathways in a clinical diagnosis group

The DA analysis of gut microbiome functional pathways, stratified by species within each pathway, identified 116 distinct pathways that differ between individuals with AD and CU individuals (**Table S3**). Among 116 distinct pathways, we focused our analysis on pathways that only showed abundance in either the Top (more abundant in AD) or the Bottom (less abundant in AD) group. Among pathway features only with either the Top (15 pathways) or the Bottom (6 pathways) group, the log ratios of Top/Bottom features were shown to be significantly different between AD and CU (**Figure 6A**). Furthermore, gut microbiome taxonomic features that were associated with pathway features (36 features) only with either the Top or Bottom group were visualized with each pathway category (**Figure 6B**). For example, a pathway, naphthalene degradation, was one of the Bottom pathways, and microbes associated with this pathway were species *Turicibacter sanguinis*, *Bifidobacterium angulatum*, and *Lactococcus lactis* (**Figure 6B**). Another example in the Top pathway is benzoate degradation which is associated with microbes including *Anaerostipes caccae*, *Bacteroides finegoldii*, and *Bacteroides thetaiotaomicron* (**Figure 6B**).

RPCA on microbiome pathway features (36 features from DA analysis) visualized with a biplot indicated a significant separation between the clinical diagnosis group (AD and CU, *P* value = .004) (**Figure 6C**). Microbial features that belonged to the Top group indicated by the red vector directed towards many AD subjects indicated by the orange dots. Microbial features that belonged to the Bottom group indicated by the green vector directed towards many CU subjects indicated by the blue dots. For instance, multiple pathways from species *Bacteroides thetaiotaomicron* pointed towards the AD group suggesting a potentially stronger association between the Top features and AD group (**Figure 6C**). On the other hand, pathways from species *Turicibacter sanguinis*, *Bifidobacterium angulatum*, and *Lactococcus lactis*, which belonged to the Bottom group, pointed towards the CU group or showed different directions compared to the Top features suggesting a potentially weaker association between the Bottom features and AD group (**Figure 6C**).

3.7 Associations between gut microbiome compositional and functional features in clinical diagnosis group and CSF biomarkers of AD and related pathologies

Associations between gut microbiome features (composition and function) and CSF biomarkers of AD and related pathologies were performed as described in the 'Statistical analysis' section of the 'Methods' (**Figure 7**).

Overall, in the association between gut microbiome compositional features and CSF biomarkers of AD and related pathologies, most species that were more abundant in AD compared to CU individuals were positively correlated with CSF biomarkers. Conversely, species that were less abundant in AD were generally negatively associated with CSF biomarkers. CSF biomarkers for AD and related pathologies included in the analysis were amyloid pathology ($A\beta_{42}/A\beta_{40}$), tau pathophysiology ($pTau_{181}$ and tTau), neurodegeneration (NfL), synaptic dysfunction and injury (neurogranin and α-synuclein), inflammation (IL-6), and glial activation (S100B, GFAP, YKL-40, and sTREM2) (**Figure 7A**).

Species that were more abundant in AD were generally positively associated with CSF biomarkers. For example, *Nanogingivalis gingivitcus*, more abundant in AD, was positively associated with S100B, neurogranin, $pTau_{181}$, and tTau. *Fusobacterium_A mortiferum* was positively correlated with neurogranin, $pTau_{181}$, tTau, and α-synuclein, and negatively associated with CSF amyloid ($A\beta_{42}/A\beta_{40}$). *Fusobacterium animalis* was positively associated with neurogranin, $pTau_{181}$, tTau, and α-synuclein. *CAG-1031 sp000431215*, a species within the Bacteroidetes phylum, was positively correlated with NfL, YKL-40, $pTau_{181}$, tTau, and α-synuclein. *Berrvella sp001552935* was positively associated with YKL-40, sTREM2, tTau, and α-synuclein. Additionally, *Lactobacillus acidophilus* and *Bifidobacterium vaginale* were positively associated with S100B, *CAG-977 sp000434295* was associated with $pTau_{181}$ and tTau, *Fusobacterium nucleatum* was associated with tTau, *Limosilactobacillus vaginalis* and *Collinsella tanakaei* were associated with $pTau_{181}$, and *CAG-177 sp000431775* was associated with IL-6.

Species that were less abundant in AD were generally negatively associated with CSF biomarkers. Species *SFMI01 sp004556155*, *Turicibacter sanquinis*, and *Dialister hominis*, all within the Firmicutes phylum, were negatively associated with neurogranin, $pTau_{181}$, tTau, and α-synuclein. *UBA5809 sp002417965*, another Firmicutes species, was also negatively associated with neurogranin, $pTau_{181}$, tTau, and α-synuclein, as well as sTREM2. *UBA11524 sp000437595*, another Firmicutes species, was negatively associated with NfL. *Cryptobacteroides sp900544195* and *Cryptobacteroides sp000432515*, both species under phylum Bacteroidetes, were negatively associated with S100B.

In the association between gut microbiome functional features and CSF biomarkers of AD and related pathologies, multiple microbial pathways more abundant in AD compared to CU showed a tendency to positively correlate with the CSF biomarkers, whereas pathways less abundant in AD compared to CU showed a tendency to have negative associations with the CSF biomarkers (**Figure 7B**). It should be noted that a lower $A\beta_{42}/A\beta_{40}$ ratio is associated with a higher risk of having AD pathology whereas higher levels of the rest of the CSF biomarkers are associated with a higher risk of having AD pathology. The same categories of CSF biomarkers for AD and related pathologies were included in the analysis including $A\beta_{42}/A\beta_{40}$, $pTau_{181}$, tTau, IL-6, NfL, neurogranin, α-synuclein, S100B, GFAP, YKL-40, and sTREM2.

Microbial functional features in the Top group showed overall positive associations with CSF biomarkers with the exception of $A\beta_{42}/A\beta_{40}$. Multiple *Bacteroides* spp. and their related pathways were positively associated with several CSF biomarkers including NfL, neurogranin, α-synuclein, $pTau_{181}$, and tTau. *Bacteroides thetaiotaomicron* and its associated pathways including benzoate degradation, ubiquinone and other terpenoid-quinone biosynthesis, biosynthesis of various plant secondary metabolites, inositol phosphate metabolism, lipoic acid metabolism, biosynthesis of various antibiotics, beta-alanine metabolism, carbapenem biosynthesis, neomycin, kanamycin and gentamicin biosynthesis, polyketide sugar unit biosynthesis, ascorbate and aldarate metabolism, and taurine and hypotaurine metabolism had generally positive relationship with CSF biomarkers including NfL, YKL-40, neurogranin, α-synuclein, $pTau_{181}$, and tTau, and negative relationship with IL-6. *Collinsella stercoris* and polyketide sugar unit biosynthesis pathway showed positive correlation with GFAP and sTREM2, and negative correlation with $A\beta_{42}/A\beta_{40}$. *Collinsella stercoris* and O-antigen repeat unit biosynthesis pathway showed negative correlation with $A\beta_{42}/A\beta_{40}$.

Microbial functional features in the Bottom group showed overall negative associations with CSF biomarkers for AD and related pathologies. Two pathways, ether lipid metabolism and alpha-linolenic acid metabolism, related to *Parabacteroides merdae*, a species more abundant in CU group were associated with lower CSF $A\beta_{42}/A\beta_{40}$. It implies that higher abundance of these pathways of *Parabacteroides merdae* in CU individuals is associated with more brain amyloid. Moreover, bacterial chemotaxis pathway from *Coprococcus eutactus* was negatively associated with NfL and YKL-40, and naphthalene degradation pathway from *Turicibacter sanguinis* was negatively associated with α-synuclein, $pTau_{181}$, and tTau.

4 DISCUSSION

In this study, we compared gut microbiome composition and function between several AD-relevant groups, including those with a clinical diagnosis, differential amyloid status, and *APOE ε4* carrier status. The objective was to determine the association of gut microbiome features that are differentially abundant in AD dementia and determine association with CSF biomarkers of AD and related pathological features, to potentially identify gut microbial features associated with AD.

Alpha and beta diversity analysis was performed between groups of each clinical diagnosis, amyloid status, and *APOE ε4* status groups. Prior studies have found that alpha and beta diversities do not differ between AD vs CU[61,62] and A+ vs A−[63] while other studies showed significant differences in alpha and beta diversity indices in humans[4,7] and mice.[64–66]

The DA analysis in gut microbiome composition at each taxonomic level using BIRDMAn was performed in AD-related groups. Similar results were reported in other studies[6,67] while opposite findings were also found, where fewer Bacteroidetes and more Firmicutes were reported in MCI compared to healthy controls and fewer genera *Bacteroides* and *Alistipes* and more genus *Bifidobacterium* were found in AD compared to health controls.[68,69] A meta-analysis of gut microbiome compositional differences in AD across studies between 2000 to 2021 demonstrated similar outcomes measured by overall pooled effect size at each taxonomic level.[7]

Discrepancies between studies may be due to differences in sample size, population variation, disease heterogeneity, sequencing method, and confounding factors.[70] Our study addresses these discrepancies through robust methodologies. Firstly, we utilized shotgun metagenomic sequencing, which provides more comprehensive taxonomic and functional profiling of microbial communities compared to 16S rRNA sequencing.[71] Additionally, we employed advanced statistical methodologies that have been shown to be replicable across multiple cohorts.[52] Lastly, we validated our findings with a larger cohort from the AGMP, which significantly enhances the reliability and generalizability of our result. Our validation of the DA analysis in a larger cohort largely recapitulates what we found in the smaller sample, confirming that alterations in gut microbiome composition are present in AD dementia.

To further determine co-occurring gut microbes among clinical diagnosis, amyloid status, and *APOE ε4* status groups, a co-occurrence analysis was performed on differentially abundant microbes in each group. Investigating co-occurring taxonomic features may be useful in the examination of gut microbiota that could potentially coexist and contribute to AD pathology related to amyloid pathology or *APOE ε4* pathology which are phenotypic and genotypic pathological signatures of AD. Studies have shown gut microbiota differences between CU+ (Aβ-positive) and CU− (Aβ-negative).[8,11,72] One of the studies showed that Phylum Bacteroidetes, class Bacteroidia, and order Bacteroidales were enriched in CN+ and phylum Firmicutes, class Clostridia, order Clostridiales, families *Lachnospiraceae* and *Ruminococcaceae*, and genera *Faecalibacterium* and *Bilophila* were enriched in CN−.[11] Higher abundance of genera *Faecalibacterium* and *Bilophila* was negatively correlated with the global brain Aβ burden.[11] Another study explored gut microbiome taxa which are pro-inflammatory with blood inflammation markers.[73] Genus *Escherichia*/*Shigella* was significantly more abundant in A+ compared with A− individuals. Genus *Escherichia*/*Shigella* was correlated positively with peripheral inflammatory cytokines in individuals with cognitive impairment and brain amyloidosis.[73]

Taken together, results from our study and other studies suggest that diverse and distinct gut microbiota taxonomic composition is altered in AD dementia, among individuals with preclinical AD, and individuals with genetic risk for AD. However, studies are limited to taxonomic and compositional associations and the determination of microbial functions in AD pathogenesis is needed to better understand the role of specific gut microbes and their functions in the progression of AD.

This study further examined the functional pathways of gut microbiome in a clinical diagnosis group between AD and CU. Gut microbiome pathways and associated species that are differentially abundant between AD and CU were determined. We found 116 distinct pathways between AD and CU. Among 116 KO pathway features, 21 pathways had associations either with AD (Top) or CU (Bottom) group. The log ratios of these Top/Bottom microbial pathway features between AD and CU were significantly different. Interestingly, species that were associated with these microbial pathways were mostly *Bacteroides* spp. (*B*. *finegoldii*, *B*. *thetaiotaomicron*, and *B*. *ovatus*) under phlyum Bacteroidota in the Top group. Multiple studies have reported the association between *Bacteroides* and AD.[4,74,75] Administration of *Bacteroides fragilis* to AD mice increased Aβ plaques and inhibition of microglial clearance of Aβ was observed after introduction to *B*. *fragilis*.[76] Another study showed the role of *B*. *fragilis* in

AD pathology in mice.[77] Studies have suggested that genus *Bacteroides* to be dominant in older adults compared with healthy and younger controls.[78,79] However, contrasting findings have been reported related to *Bacteroides*[8,80] and further strain-specific studies are needed to understand the role of *Bacteroides* in AD pathology.

Additionally, RPCA showed a distinct significant separation between AD and CU groups. RPCA is known to handle sparse and high-dimensional datasets and is sensitive to datasets with outliers.[54] Microbiome datasets are often sparse and zero-inflated, thus we employed RPCA to identify microbiome features that could explain the separation between groups. Consistent with the DA analysis, RPCA showed microbial pathways that are more abundant in AD (Top) were more associated with AD dementia, whereas microbial pathways less abundant in AD (Bottom) were less associated with AD dementia.

To determine whether distinct microbial features in AD and CU correlate with CSF biomarkers of AD and related pathologies, the relationship between CSF biomarkers and each compositional and functional gut microbiome feature was explored using the OLS regression model.

Key microbiome species, particularly *Fusobacterium nucleatum*, *Fusobacterium animalis*, and *Nanogingivalis gingivitcus*, identified as commonly more abundant between AD and A+, were associated with more intense tau pathophysiology ($pTau_{181}$ and tTau) and/or synaptic dysfunction and injury (neurogranin and α-synuclein). Interestingly, the species *Fusobacterium nucleatum* is an oral bacteria often associated with cavity and periodontal diseases as well as colorectal cancer.[81,82] *Fusobacterium nucleatum* produces lipopolysaccharides (LPS) that induce microglial activation with elevated expression of proinflammatory cytokines.[83] In prior studies using the 5XFAD mouse model, the mRNA expression levels of the same proinflammatory cytokines as well as numbers of microglia in the mice brain were increased after *Fusobacterium nucleatum* infection.[83] Moreover, enhanced Aβ accumulation, tau protein phosphorylation, and memory impairment were observed in 5XFAD mice compared to controls.[83] The oral infection of *Fusobacterium nucleatum* in AD-like periodontitis rats exhibited increased accumulation of Aβ and $pTau_{181}$ expression in the brain.[84] Although these results propose valuable mechanistic backgrounds for *Fusobacterium nucleatum* and AD, further investigation in humans is needed.

The species *Dialister hominis,* a microbe that co-occurred between CU and A− displayed a negative correlation with AD pathology ($pTau_{181}$), neuronal damage (tTau), and synaptic dysfunction and injury (neurogranin and α-synuclein). These findings are similar to previous works which identified genus *Dialister* (less in AD) to be more abundant in CU individuals.[85,86] Another species *Turicibacter sanguinis* which was a microbe that co-occurred between CU and *APOE ε4*− showed a negative correlation with $pTau_{181}$, tTau, neurogranin, and α-synuclein. In animal models for AD, *Turicibacter sanguinis* is reported to be less abundant in AD compared to controls.[87,88] In humans, *Turicibacter* was observed to be less abundant in individuals with AD.[4] However, studies on the role of species specific to *Dialister hominis* and *Turicibacter sanguinis* in AD pathology are scarce.

This result indicates that microbiota compositional features in CU are related to lower levels of AD pathology whereas microbiota features in AD are related to higher levels of AD pathology, suggesting overall microbiota composition in people with AD may be vulnerable to

development or progression of AD compared to CU individuals. While these results support a relationship between gut microbiome composition and AD pathology, further investigation into these mechanisms is required to find a causal relationship.

Multiple *Bacteroides* spp. and their related functional pathways more abundant in AD were associated with greater AD pathology represented in CSF biomarkers of AD and related pathologies. Biomarkers including neurodegeneration (NfL), synaptic dysfunction and injury (neurogranin and α-synuclein), and tau pathophysiology ($pTau_{181}$ and tTau) showed a positive relationship with *Bacteroides thetaiotaomicron* and their functions. Studies have linked the abundance of *Bacteroides thetaiotaomicron* with AD. The abundance of *B*. *thetaiotaomicron* was significantly higher in AD mice and was related to poorer spatial learning.[89] Increased abundance of *B*. *thetaiotaomicron* was reported in AD participants.[90,91] However, in a non-AD model, *B*. *thetaiotaomicron* was suggested to regulate enteric neuronal cell populations and neurogenic function.

Although evidence related to these microbial functions is limited, these results suggest that alterations in gut microbiome composition and function are related to AD pathological markers measured in CSF.

The main limitation of our study is the small number of cognitively impaired participants relative to CU participants. The sample size decreased after matching clinical measurements, gut microbiome data, and presence of CSF biomarkers. The resulting low statistical power may have led to losing significance after multiple test corrections for association analyses between gut microbiome features and CSF biomarkers. A similar challenge is the inclusion of cognitively impaired individuals in both the A+ and *APOE ε4* groups. Excluding these individuals reduced the sample sizes, resulting in low statistical power. Future studies should aim to collect sufficient samples to separate these groups, allowing for a clearer distinction between disease effects and symptom effects. Moreover, due to the cross-sectional approach, it is difficult to capture the longitudinal changes over time considering the progression of AD for each individual. We included the ADRC validation cohort to account for differences in gut microbiome composition across diverse populations, however, due to the limitation of the availability of biomarkers matched with fecal samples, we were not able to test associations with CSF biomarkers in the validation cohort. Additionally, the results are correlational, and further mechanistic studies are needed to find causal relationships between gut microbiome features and biomarkers for AD pathology. Finally, other environmental factors (exposome) which may impact the gut microbiome and which contribute to AD risk require additional study in the future.

5 CONCLUSIONS

This study suggests that gut microbiome composition and function differ between people with AD dementia and CU individuals. Beta diversity indices differed among AD-related groups: diagnosis (AD vs CU), amyloid (A+ vs A−), and *APOE ε4* (*APOE ε4*+ vs *APOE ε4*−) groups, indicating that the gut microbiome diversity varies between each group. Multiple gut microbes at each taxonomic level including phylum, family, genus, and species were differentially abundant across AD groups. Co-occurring gut microbes across AD-related groups were determined,

many of which showed associations with CSF biomarkers for AD and related pathologies. Microbial functional pathways were differentially abundant between AD and CU, which were correlated with AD pathology markers measured in CSF. These findings identify specific targets for stratifying key gut microbes and microbial pathways that may be related to AD pathology. Further investigation on metabolomic changes as well as exposome and host genome that may be mediating the interconnectome between the gut microbiome and AD pathology is needed.

References

1. Sonnenburg JL, Bäckhed F. Diet–microbiota interactions as moderators of human metabolism. *Nature*. 2016;535(7610):56-64. doi:10.1038/nature18846

2. Desai MS, Seekatz AM, Koropatkin NM, et al. A Dietary Fiber-Deprived Gut Microbiota Degrades the Colonic Mucus Barrier and Enhances Pathogen Susceptibility. *Cell*. 2016;167(5):1339-1353.e21. doi:10.1016/j.cell.2016.10.043

3. Lee WJ, Hase K. Gut microbiota–generated metabolites in animal health and disease. *Nat Chem Biol*. 2014;10(6):416-424. doi:10.1038/nchembio.1535

4. Vogt NM, Kerby RL, Dill-McFarland KA, et al. Gut microbiome alterations in Alzheimer's disease. *Sci Rep*. 2017;7:13537. doi:10.1038/s41598-017-13601-y

5. Zhuang ZQ, Shen LL, Li WW, et al. Gut Microbiota is Altered in Patients with Alzheimer's Disease. *Journal of Alzheimer's Disease*. 2018;63(4):1337-1346. doi:10.3233/JAD-180176

6. Liu P, Wu L, Peng G, et al. Altered microbiomes distinguish Alzheimer's disease from amnestic mild cognitive impairment and health in a Chinese cohort. *Brain Behav Immun*. 2019;80:633-643. doi:10.1016/j.bbi.2019.05.008

7. Hung CC, Chang CC, Huang CW, Nouchi R, Cheng CH. Gut microbiota in patients with Alzheimer's disease spectrum: a systematic review and meta-analysis. *Aging (Albany NY)*. 2022;14(1):477-496. doi:10.18632/aging.203826

8. Ferreiro AL, Choi J, Ryou J, et al. Gut microbiome composition may be an indicator of preclinical Alzheimer's disease. *Science Translational Medicine*. 2023;15(700):eabo2984. doi:10.1126/scitranslmed.abo2984

9. Vogt NM, Romano KA, Darst BF, et al. The gut microbiota-derived metabolite trimethylamine N-oxide is elevated in Alzheimer's disease. *Alzheimer's Research & Therapy*. 2018;10(1):124. doi:10.1186/s13195-018-0451-2

10. Nabizadeh F, Valizadeh P, Fallahi MS, Alzheimer's disease Neuroimaging Initiative. Bile acid profile associated with CSF and PET biomarkers in Alzheimer's disease. *Aging Clin Exp Res*. 2024;36(1):62. doi:10.1007/s40520-024-02729-3

11. Sheng C, Yang K, He B, Du W, Cai Y, Han Y. Combination of gut microbiota and plasma amyloid-β as a potential index for identifying preclinical Alzheimer's disease: a cross-sectional analysis from the SILCODE study. *Alzheimer's Research & Therapy*. 2022;14(1):35. doi:10.1186/s13195-022-00977-x

12. Sochocka M, Donskow-Łysoniewska K, Diniz BS, Kurpas D, Brzozowska E, Leszek J. The Gut Microbiome Alterations and Inflammation-Driven Pathogenesis of Alzheimer's Disease—a Critical Review. *Mol Neurobiol*. 2019;56(3):1841-1851. doi:10.1007/s12035-018-1188-4

13. Heston MB, Hanslik KL, Zarbock KR, et al. Gut inflammation associated with age and Alzheimer's disease pathology: a human cohort study. *Sci Rep*. 2023;13(1):18924. doi:10.1038/s41598-023-45929-z

14. Heintz-Buschart A, Wilmes P. Human Gut Microbiome: Function Matters. *Trends in Microbiology*. 2018;26(7):563-574. doi:10.1016/j.tim.2017.11.002

15. Chernikova MA, Flores GD, Kilroy E, Labus JS, Mayer EA, Aziz-Zadeh L. The Brain-Gut-Microbiome System: Pathways and Implications for Autism Spectrum Disorder. *Nutrients*. 2021;13(12):4497. doi:10.3390/nu13124497

16. Kenna JE, Chua EG, Bakeberg M, et al. Changes in the Gut Microbiome and Predicted Functional Metabolic Effects in an Australian Parkinson's Disease Cohort. *Front Neurosci*. 2021;15. doi:10.3389/fnins.2021.756951

17. Ananthakrishnan AN, Luo C, Yajnik V, et al. Gut Microbiome Function Predicts Response to Anti-integrin Biologic Therapy in Inflammatory Bowel Diseases. *Cell Host & Microbe*. 2017;21(5):603-610.e3. doi:10.1016/j.chom.2017.04.010

18. Paley EL. Discovery of Gut Bacteria Specific to Alzheimer's Associated Diseases is a Clue to Understanding Disease Etiology: Meta-Analysis of Population-Based Data on Human Gut Metagenomics and Metabolomics. *Journal of Alzheimer's Disease*. 2019;72(1):319-355. doi:10.3233/JAD-190873

19. Laske C, Müller S, Preische O, et al. Signature of Alzheimer's Disease in Intestinal Microbiome: Results From the AlzBiom Study. *Front Neurosci*. 2022;16. doi:10.3389/fnins.2022.792996

20. Li J, Zhu S, Wang Y, et al. Metagenomic association analysis of cognitive impairment in community-dwelling older adults. *Neurobiology of Disease*. 2023;180:106081. doi:10.1016/j.nbd.2023.106081

21. Johnson SC, Koscik RL, Jonaitis EM, et al. The Wisconsin Registry for Alzheimer's Prevention: A review of findings and current directions. *Alzheimers Dement (Amst)*. 2018;10:130-142. doi:10.1016/j.dadm.2017.11.007

22. Darst BF, Koscik RL, Racine AM, et al. Pathway-specific polygenic risk scores as predictors of β-amyloid deposition and cognitive function in a sample at increased risk for Alzheimer's disease. *J Alzheimers Dis*. 2017;55(2):473-484. doi:10.3233/JAD-160195

23. Albert MS, DeKosky ST, Dickson D, et al. The diagnosis of mild cognitive impairment due to Alzheimer's disease: Recommendations from the National Institute on Aging-Alzheimer's Association workgroups on diagnostic guidelines for Alzheimer's disease. *Alzheimer's & Dementia*. 2011;7(3):270-279. doi:10.1016/j.jalz.2011.03.008

24. McKhann GM, Knopman DS, Chertkow H, et al. The diagnosis of dementia due to Alzheimer's disease: recommendations from the National Institute on Aging-Alzheimer's Association workgroups on diagnostic guidelines for Alzheimer's disease. *Alzheimers Dement*. 2011;7(3):263-269. doi:10.1016/j.jalz.2011.03.005

25. Betthauser TJ, Koscik RL, Jonaitis EM, et al. Amyloid and tau imaging biomarkers explain cognitive decline from late middle-age. *Brain*. 2020;143(1):320-335. doi:10.1093/brain/awz378

776 26. Van Hulle C, Jonaitis EM, Betthauser TJ, et al. An examination of a novel multipanel of CSF
777 biomarkers in the Alzheimer's disease clinical and pathological continuum. *Alzheimer's &*
778 *Dementia*. 2021;17(3):431-445. doi:10.1002/alz.12204

779 27. Marotz C, Amir A, Humphrey G, Gaffney J, Gogul G, Knight R. DNA extraction for
780 streamlined metagenomics of diverse environmental samples. *BioTechniques*.
781 2017;62(6):290-293. doi:10.2144/000114559

782 28. Glenn TC, Nilsen RA, Kieran TJ, et al. Adapterama I: universal stubs and primers for 384
783 unique dual-indexed or 147,456 combinatorially-indexed Illumina libraries (iTru & iNext).
784 *PeerJ*. 2019;7:e7755. doi:10.7717/peerj.7755

785 29. Sanders JG, Nurk S, Salido RA, et al. Optimizing sequencing protocols for leaderboard
786 metagenomics by combining long and short reads. *Genome Biology*. 2019;20(1):226.
787 doi:10.1186/s13059-019-1834-9

788 30. Marotz C, Cavagnero KJ, Song SJ, et al. Evaluation of the Effect of Storage Methods on
789 Fecal, Saliva, and Skin Microbiome Composition. *mSystems*. 2021;6(2):e01329-20.
790 doi:10.1128/mSystems.01329-20

791 31. Sepich-Poore GD, McDonald D, Kopylova E, et al. Robustness of cancer microbiome
792 signals over a broad range of methodological variation. *Oncogene*. 2024;43(15):1127-1148.
793 doi:10.1038/s41388-024-02974-w

794 32. Chen S, Zhou Y, Chen Y, Gu J. fastp: an ultra-fast all-in-one FASTQ preprocessor.
795 *Bioinformatics*. 2018;34(17):i884-i890. doi:10.1093/bioinformatics/bty560

796 33. Liao WW, Asri M, Ebler J, et al. A draft human pangenome reference. *Nature*.
797 2023;617(7960):312-324. doi:10.1038/s41586-023-05896-x

798 34. Rhie A, Nurk S, Cechova M, et al. The complete sequence of a human Y chromosome.
799 *Nature*. 2023;621(7978):344-354. doi:10.1038/s41586-023-06457-y

800 35. Schneider VA, Graves-Lindsay T, Howe K, et al. Evaluation of GRCh38 and de novo
801 haploid genome assemblies demonstrates the enduring quality of the reference assembly.
802 *Genome Res*. 2017;27(5):849-864. doi:10.1101/gr.213611.116

803 36. Li H. New strategies to improve minimap2 alignment accuracy. *Bioinformatics*.
804 2021;37(23):4572-4574. doi:10.1093/bioinformatics/btab705

805 37. Danecek P, Bonfield JK, Liddle J, et al. Twelve years of SAMtools and BCFtools.
806 *Gigascience*. 2021;10(2):giab008. doi:10.1093/gigascience/giab008

807 38. Edwards JA, Edwards RA. Fastq-pair: efficient synchronization of paired-end fastq files.
808 Published online February 19, 2019:552885. doi:10.1101/552885

809 39. Tange O. *Gnu Parallel 2018*. [object Object]; 2018. doi:10.5281/ZENODO.1146014

810 40. Köster J. Rust-Bio: a fast and safe bioinformatics library. *Bioinformatics*. 2016;32(3):444-
811 446. doi:10.1093/bioinformatics/btv573

41. Gonzalez A, Navas-Molina JA, Kosciolek T, et al. Qiita: rapid, web-enabled microbiome meta-analysis. *Nat Methods*. 2018;15(10):796-798. doi:10.1038/s41592-018-0141-9

42. Zhu Q, Huang S, Gonzalez A, et al. Phylogeny-Aware Analysis of Metagenome Community Ecology Based on Matched Reference Genomes while Bypassing Taxonomy. *mSystems*. 2022;7(2):e00167-22. doi:10.1128/msystems.00167-22

43. Hakim D, Wandro S, Zengler K, et al. Zebra: Static and Dynamic Genome Cover Thresholds with Overlapping References. *mSystems*. 2022;7(5):e0075822. doi:10.1128/msystems.00758-22

44. Bolyen E, Rideout JR, Dillon MR, et al. Reproducible, interactive, scalable and extensible microbiome data science using QIIME 2. *Nat Biotechnol*. 2019;37(8):852-857. doi:10.1038/s41587-019-0209-9

45. Betthauser TJ, Cody KA, Zammit MD, et al. In Vivo Characterization and Quantification of Neurofibrillary Tau PET Radioligand 18F-MK-6240 in Humans from Alzheimer Disease Dementia to Young Controls. *Journal of Nuclear Medicine*. 2019;60(1):93-99. doi:10.2967/jnumed.118.209650

46. Shannon CE. A mathematical theory of communication. *The Bell System Technical Journal*. 1948;27(3):379-423. doi:10.1002/j.1538-7305.1948.tb01338.x

47. Pielou EC. The measurement of diversity in different types of biological collections. *Journal of Theoretical Biology*. 1966;13:131-144. doi:10.1016/0022-5193(66)90013-0

48. Faith DP. Conservation evaluation and phylogenetic diversity. *Biological Conservation*. 1992;61(1):1-10. doi:10.1016/0006-3207(92)91201-3

49. Sørensen T, Sørensen T, Biering-Sørensen T, Sørensen T, Sorensen JT. *A Method of Establishing Group of Equal Amplitude in Plant Sociobiology Based on Similarity of Species Content and Its Application to Analyses of the Vegetation on Danish Commons*. Vol 5. København□: I kommission hos E. Munksgaard; 1948. https://api.semanticscholar.org/CorpusID:135206594

50. Lozupone CA, Hamady M, Kelley ST, Knight R. Quantitative and Qualitative β Diversity Measures Lead to Different Insights into Factors That Structure Microbial Communities. *Applied and Environmental Microbiology*. 2007;73(5):1576-1585. doi:10.1128/AEM.01996-06

51. Lozupone C, Knight R. UniFrac: a New Phylogenetic Method for Comparing Microbial Communities. *Applied and Environmental Microbiology*. 2005;71(12):8228-8235. doi:10.1128/AEM.71.12.8228-8235.2005

52. Rahman G, Morton JT, Martino C, et al. BIRDMAn: A Bayesian differential abundance framework that enables robust inference of host-microbe associations. *bioRxiv*. Published online February 2, 2023:2023.01.30.526328. doi:10.1101/2023.01.30.526328

53. Mao X, Cai T, Olyarchuk JG, Wei L. Automated genome annotation and pathway identification using the KEGG Orthology (KO) as a controlled vocabulary. *Bioinformatics*. 2005;21(19):3787-3793. doi:10.1093/bioinformatics/bti430

851 54. Martino C, Morton JT, Marotz CA, et al. A Novel Sparse Compositional Technique Reveals
852 Microbial Perturbations. *mSystems*. 2019;4(1):10.1128/msystems.00016-19.
853 doi:10.1128/msystems.00016-19

854 55. Anderson MJ. Permutational Multivariate Analysis of Variance (PERMANOVA). In: *Wiley*
855 *StatsRef: Statistics Reference Online*. John Wiley & Sons, Ltd; 2017:1-15.
856 doi:10.1002/9781118445112.stat07841

857 56. Pedregosa F, Varoquaux G, Gramfort A, et al. Scikit-learn: Machine Learning in Python.
858 *Journal of Machine Learning Research*. 2011;12(85):2825-2830. Accessed August 12,
859 2024. http://jmlr.org/papers/v12/pedregosa11a.html

860 57. Virtanen P, Gommers R, Oliphant TE, et al. SciPy 1.0: fundamental algorithms for scientific
861 computing in Python. *Nat Methods*. 2020;17(3):261-272. doi:10.1038/s41592-019-0686-2

862 58. van der Walt S, Colbert SC, Varoquaux G. The NumPy Array: A Structure for Efficient
863 Numerical Computation. *Computing in Science & Engineering*. 2011;13(2):22-30.
864 doi:10.1109/MCSE.2011.37

865 59. Hunter JD. Matplotlib: A 2D Graphics Environment. *Computing in Science & Engineering*.
866 2007;9(3):90-95. doi:10.1109/MCSE.2007.55

867 60. Waskom ML. seaborn: statistical data visualization. *Journal of Open Source Software*.
868 2021;6(60):3021. doi:10.21105/joss.03021

869 61. Hou M, Xu G, Ran M, Luo W, Wang H. APOE-ε4 Carrier Status and Gut Microbiota
870 Dysbiosis in Patients With Alzheimer Disease. *Front Neurosci*. 2021;15.
871 doi:10.3389/fnins.2021.619051

872 62. Kaiyrlykyzy A, Kozhakhmetov S, Babenko D, et al. Study of gut microbiota alterations in
873 Alzheimer's dementia patients from Kazakhstan. *Sci Rep*. 2022;12:15115.
874 doi:10.1038/s41598-022-19393-0

875 63. Jung JH, Kim G, Byun MS, et al. Gut microbiome alterations in preclinical Alzheimer's
876 disease. *PLOS ONE*. 2022;17(11):e0278276. doi:10.1371/journal.pone.0278276

877 64. Zajac DJ, Green SJ, Johnson LA, Estus S. APOE genetics influence murine gut
878 microbiome. *Sci Rep*. 2022;12(1):1906. doi:10.1038/s41598-022-05763-1

879 65. Tran TTT, Corsini S, Kellingray L, et al. APOE genotype influences the gut microbiome
880 structure and function in humans and mice: relevance for Alzheimer's disease
881 pathophysiology. *FASEB J*. 2019;33(7):8221-8231. doi:10.1096/fj.201900071R

882 66. Xiao-hang Q, Si-yue C, Hui-dong T. Multi-strain probiotics ameliorate Alzheimer's-like
883 cognitive impairment and pathological changes through the AKT/GSK-3β pathway in
884 senescence-accelerated mouse prone 8 mice. *Brain, Behavior, and Immunity*. 2024;119:14-
885 27. doi:10.1016/j.bbi.2024.03.031

886 67. Liu P, Jia XZ, Chen Y, et al. Gut microbiota interacts with intrinsic brain activity of patients
887 with amnestic mild cognitive impairment. *CNS Neuroscience & Therapeutics*.
888 2021;27(2):163-173. doi:10.1111/cns.13451

68. Li B, He Y, Ma J, et al. Mild cognitive impairment has similar alterations as Alzheimer's disease in gut microbiota. *Alzheimers Dement*. 2019;15(10):1357-1366. doi:10.1016/j.jalz.2019.07.002

69. Nagpal R, Neth BJ, Wang S, Craft S, Yadav H. Modified Mediterranean-ketogenic diet modulates gut microbiome and short-chain fatty acids in association with Alzheimer's disease markers in subjects with mild cognitive impairment. *eBioMedicine*. 2019;47:529-542. doi:10.1016/j.ebiom.2019.08.032

70. Li Z, Zhou J, Liang H, et al. Differences in Alpha Diversity of Gut Microbiota in Neurological Diseases. *Front Neurosci*. 2022;16. doi:10.3389/fnins.2022.879318

71. Jovel J, Patterson J, Wang W, et al. Characterization of the Gut Microbiome Using 16S or Shotgun Metagenomics. *Front Microbiol*. 2016;7. doi:10.3389/fmicb.2016.00459

72. Verhaar BJH, Hendriksen HMA, de Leeuw FA, et al. Gut Microbiota Composition Is Related to AD Pathology. *Front Immunol*. 2022;12. doi:10.3389/fimmu.2021.794519

73. Cattaneo A, Cattane N, Galluzzi S, et al. Association of brain amyloidosis with pro-inflammatory gut bacterial taxa and peripheral inflammation markers in cognitively impaired elderly. *Neurobiology of Aging*. 2017;49:60-68. doi:10.1016/j.neurobiolaging.2016.08.019

74. Haran JP, Bhattarai SK, Foley SE, et al. Alzheimer's Disease Microbiome Is Associated with Dysregulation of the Anti-Inflammatory P-Glycoprotein Pathway. *mBio*. 2019;10(3):10.1128/mbio.00632-19. doi:10.1128/mbio.00632-19

75. Cammann D, Lu Y, Cummings MJ, et al. Genetic correlations between Alzheimer's disease and gut microbiome genera. *Sci Rep*. 2023;13(1):5258. doi:10.1038/s41598-023-31730-5

76. Wasén C, Beauchamp LC, Vincentini J, et al. Bacteroidota inhibit microglia clearance of amyloid-beta and promote plaque deposition in Alzheimer's disease mouse models. *Nat Commun*. 2024;15:3872. doi:10.1038/s41467-024-47683-w

77. Xia Y, Xiao Y, Wang ZH, et al. Bacteroides Fragilis in the gut microbiomes of Alzheimer's disease activates microglia and triggers pathogenesis in neuronal C/EBPβ transgenic mice. *Nat Commun*. 2023;14(1):5471. doi:10.1038/s41467-023-41283-w

78. Claesson MJ, Cusack S, O'Sullivan O, et al. Composition, variability, and temporal stability of the intestinal microbiota of the elderly. *Proceedings of the National Academy of Sciences*. 2011;108(supplement_1):4586-4591. doi:10.1073/pnas.1000097107

79. Wilmanski T, Diener C, Rappaport N, et al. Gut microbiome pattern reflects healthy ageing and predicts survival in humans. *Nat Metab*. 2021;3(2):274-286. doi:10.1038/s42255-021-00348-0

80. Guo M, Peng J, Huang X, Xiao L, Huang F, Zuo Z. Gut Microbiome Features of Chinese Patients Newly Diagnosed with Alzheimer's Disease or Mild Cognitive Impairment. *Journal of Alzheimer's Disease*. 2021;80(1):299-310. doi:10.3233/JAD-201040

81. Pignatelli P, Nuccio F, Piattelli A, Curia MC. The Role of Fusobacterium nucleatum in Oral and Colorectal Carcinogenesis. *Microorganisms*. 2023;11(9):2358. doi:10.3390/microorganisms11092358

82. Zepeda-Rivera M, Minot SS, Bouzek H, et al. A distinct Fusobacterium nucleatum clade dominates the colorectal cancer niche. *Nature*. 2024;628(8007):424-432. doi:10.1038/s41586-024-07182-w

83. Wu H, Qiu W, Zhu X, et al. The Periodontal Pathogen Fusobacterium nucleatum Exacerbates Alzheimer's Pathogenesis via Specific Pathways. *Front Aging Neurosci*. 2022;14. doi:10.3389/fnagi.2022.912709

84. Yan C, Diao Q, Zhao Y, et al. Fusobacterium nucleatum infection-induced neurodegeneration and abnormal gut microbiota composition in Alzheimer's disease-like rats. *Front Neurosci*. 2022;16. doi:10.3389/fnins.2022.884543

85. Ling Z, Zhu M, Yan X, et al. Structural and Functional Dysbiosis of Fecal Microbiota in Chinese Patients With Alzheimer's Disease. *Front Cell Dev Biol*. 2021;8. doi:10.3389/fcell.2020.634069

86. Rouskas K, Mamalaki E, Ntanasi E, et al. Distinct gut microbiota profiles may characterize amyloid beta pathology and mild cognitive impairment. Published online May 3, 2024:2024.05.01.24306673. doi:10.1101/2024.05.01.24306673

87. Dunham SJB, McNair KA, Adams ED, et al. Longitudinal Analysis of the Microbiome and Metabolome in the 5xfAD Mouse Model of Alzheimer's Disease. *mBio*. 2022;13(6):e01794-22. doi:10.1128/mbio.01794-22

88. Sun P, Zhu H, Li X, et al. Comparative Metagenomics and Metabolomes Reveals Abnormal Metabolism Activity Is Associated with Gut Microbiota in Alzheimer's Disease Mice. *International Journal of Molecular Sciences*. 2022;23(19):11560. doi:10.3390/ijms231911560

89. Abraham D, Feher J, Scuderi GL, et al. Exercise and probiotics attenuate the development of Alzheimer's disease in transgenic mice: Role of microbiome. *Experimental Gerontology*. 2019;115:122-131. doi:10.1016/j.exger.2018.12.005

90. Fang Chuang Y. Altered Gut Microbiota in Dementia and Mild Cognitive Impairment in Community-Dwelling Older Adults in Taiwan. *Alzheimer's & Dementia*. 2023;19(S12):e075212. doi:10.1002/alz.075212

91. Martinelli F, Heinken A, Henning AK, et al. Whole-body metabolic modelling reveals microbiome and genomic interactions on reduced urine formate levels in Alzheimer's disease. *Sci Rep*. 2024;14(1):6095. doi:10.1038/s41598-024-55960-3

ACKNOWLEDGMENTS

This project was enabled in part by The Alzheimer Gut Microbiome Project (AGMP) and the Alzheimer's Disease Metabolomics Consortium (ADMC) funded wholly or in part by the following NIA grants thereto: U01AG061359 and U19AG063744 awarded to Dr. Kaddurah-Daouk at Duke University in partnership with multiple academic institutions. As such, the investigators within the AGMP and the ADMC, not listed specifically in this publication's author's list, provided data along with its pre-processing and prepared it for analysis, but did not participate in analysis or writing of this manuscript. A listing of AGMP Investigators can be found at alzheimergut.org/meet-the-team/. A complete listing of ADMC investigators can be found at: sites.duke.edu/adnimetab/team/. The IGM S10 grant S10 OD026929 was awarded to Dr. Rob Knight at the University of California San Diego IGM Genomics Center. This publication includes data generated at the University of California San Diego IGM Genomics Center utilizing an Illumina NovaSeq 6000 that was purchased with funding from a National Institutes of Health SIG grant (#S10 OD026929).

This work was also supported by the National Institute on Aging Grant R01AG070973 (B.B.B., F.E.R., T.K.U.), National Institute on Aging Grant R01AG083883 (T.K.U., B.B.B., F.E.R.), Vilas Early-Career Investigator Award (T.K.U.), and National Institute on Aging Grant P30AG062715 (which in part supported B.B.B., T.K.U.).

Dr. Zetterberg is a Wallenberg Scholar and a Distinguished Professor at the Swedish Research Council supported by grants from the Swedish Research Council (#2023-00356; #2022-01018 and #2019-02397), the European Union's Horizon Europe research and innovation programme under grant agreement No 101053962, Swedish State Support for Clinical Research (#ALFGBG-71320), the Alzheimer Drug Discovery Foundation (ADDF), USA (#201809-2016862), the AD Strategic Fund and the Alzheimer's Association (#ADSF-21-831376-C, #ADSF-21-831381-C, #ADSF-21-831377-C, and #ADSF-24-1284328-C), the European Partnership on Metrology, co-financed from the European Union's Horizon Europe Research and Innovation Programme and by the Participating States (NEuroBioStand, #22HLT07), the Bluefield Project, Cure Alzheimer's Fund, the Olav Thon Foundation, the Erling-Persson Family Foundation, Familjen Rönströms Stiftelse, Stiftelsen för Gamla Tjänarinnor, Hjärnfonden, Sweden (#FO2022-0270), the European Union's Horizon 2020 research and innovation programme under the Marie Skłodowska-Curie grant agreement No 860197 (MIRIADE), the European Union Joint Programme – Neurodegenerative Disease Research (JPND2021-00694), the National Institute for Health and Care Research University College London Hospitals Biomedical Research Centre, and the UK Dementia Research Institute at UCL (UKDRI-1003).

COBAS is a trademark of Roche. All other product names and trademarks are the property of their respective owners. The NeuroToolKit is a panel of exploratory prototype assays designed to robustly evaluate biomarkers associated with key pathologic events characteristic of AD and other neurological disorders, used for research purposes only and not approved for clinical use (Roche Diagnostics International Ltd, Rotkreuz, Switzerland).

CONFLICT OF INTEREST STATEMENT

Dr. Kaddurah-Daouk in an inventor on a series of patents on use of metabolomics for the diagnosis and treatment of CNS diseases and holds equity in Metabolon Inc., Chymia LLC and PsyProtix.
Dr. Rob Knight is a scientific advisory board member, and consultant for BiomeSense, Inc., has equity and receives income. He is a scientific advisory board member and has equity in GenCirq. He is a consultant for DayTwo, and receives income. He has equity in and acts as a consultant for Cybele. He is a co-founder of Biota, Inc., and has equity. He is a cofounder of Micronoma, and has equity and is a scientific advisory board member. The terms of these arrangements have been reviewed and approved by the University of California, San Diego in accordance with its conflict of interest policies.
Dr. Zetterberg has served at scientific advisory boards and/or as a consultant for Abbvie, Acumen, Alector, Alzinova, ALZPath, Amylyx, Annexon, Apellis, Artery Therapeutics, AZTherapies, Cognito Therapeutics, CogRx, Denali, Eisai, LabCorp, Merry Life, Nervgen, Novo Nordisk, Optoceutics, Passage Bio, Pinteon Therapeutics, Prothena, Red Abbey Labs, reMYND, Roche, Samumed, Siemens Healthineers, Triplet Therapeutics, and Wave, has given lectures in symposia sponsored by Alzecure, Biogen, Cellectricon, Fujirebio, Lilly, Novo Nordisk, and Roche, and is a co-founder of Brain Biomarker Solutions in Gothenburg AB (BBS), which is a part of the GU Ventures Incubator Program (outside submitted work).
Daniel McDonald is a consultant for, and has equity in, BiomeSence, Inc. The terms of this arrangement has been reviewed and approved by the University of California, San Diego in accordance with its conflict of interest polices.

CONSENT STATEMENT

All human subjects provided informed consent to participate in this study.

DATA AVAILABILITY

Samples were provided by the University of Wisconsin Alzheimer's Disease Research Center. Clinical data can be requested from the National Alzheimer's Coordinating Center (naccdata.org/).
Data will be available in the Synapse AD Knowledge Portal.
Gut Microbiome data is stored and accessible via the University of California, San Diego Qiita platform (qiita.ucsd.edu/).

Keywords

Alzheimer's disease; Gut microbiome; Composition; Function; Cerebrospinal fluid; Biomarkers; Differential abundance; Pathology

Figure legends

Figure 1

Alpha and beta diversity metrics across AD groups. (A-C) Shannon, Evenness, and Faith's PD metrics for individuals categorized by clinical diagnosis (CU vs. Dementia-AD). (D-F) Metrics for amyloid status (Negative vs. Positive). (G-I) Metrics across *APOE ε4* status (Negative vs. Positive). Each box plot is overlaid with individual data points, enhancing visualization of the data distribution within each group. Kruskal-Wallis test was used to determine statistical significance. (J-L) Differences in beta diversity metrics (Bray Curtis, Weighted UniFrac, and Unweighted UniFrac, respectively) for individuals categorized by clinical diagnosis (CU vs. Dementia-AD). (M-O) Metrics for amyloid status (Negative vs. Positive). (P-R) Metrics across *APOE ε4* status (Negative vs. Positive). Principal coordinates (PC)1 and PC2 axes represent the most variance in data. Each plot is color-coded by the respective group, highlighting the spatial distribution and clustering based on the dissimilarity indices. PERMANOVA was used to determine statistical significance.

Figure 2

Differential abundance (DA) across AD groups. Forest plots illustrating the DA of microbial features associated with AD groups. (A, D, G, and J) Contrasts in the abundance of various bacterial taxa at (A) phylum, (D) family, (G) genus, and (J) species levels between AD dementia and CU. (B, E, H, and K) The differences in abundance at these taxonomic levels between A+ and A− individuals. (C, F, I, and L) The microbial features differentially abundant between *APOE ε4+* and *APOE ε4−* groups. The x-axes quantify the log ratio of presence between groups, with values above one indicating a higher abundance in the first-mentioned group. Circles denote "Top" features, indicating a positive association with AD groups (dementia diagnosis, amyloid positivity, and *APOE ε4* positivity), whereas triangles denote "Bottom" features, indicating a negative association. The lines are color-coded by unique phylum as labeled in the legend. DA analysis was conducted using BIRDMAn.

Figure 3

Comparative analysis of top and bottom features across AD groups. Box plots comparing the distribution of log-transformed ratios of differentially abundant microbial species in relation to diagnosis, amyloid status, and *APOE ε4* status. (A-C) The log-transformed ratios of microbes for diagnosis groups (AD vs CU). (D-F) The log-transformed ratios of amyloid-related microbes (A+ vs A−). (G-I) The log-transformed ratios of *APOE ε4*-related microbes (*APOE ε4+* vs *APOE ε4−*). Each column compares the CU and AD groups (A, D, and G), A+ and A− groups (B, E, and H), and *APOE ε4+* and *APOE ε4−* groups (C, F, and I). Each panel includes a Kruskal-

Wallis test statistic and associated *P* value, indicating the statistical significance of the differences observed.

Figure 4

Venn-diagram of co-occurrence of microbial features across AD groups. The diagrams on the left column (A, C, E, and G) depict the Top (positively-associated) differentially abundant features, while those on the right column (B, D, F, and H) show the Bottom (negatively-associated) differentially abundant features. (A and B) Top and Bottom microbial phyla, respectively. These diagrams identify unique and shared phyla associated with each of the three AD groups. (C and D) Top and Bottom microbial families, respectively. These diagrams highlight the family-level microbial differences that correlate with AD diagnosis, amyloid presence, and *APOE ε4* genotype presence. (E and F) Top and Bottom microbial genera, respectively. These diagrams provide insight into the genus-level microbial composition influenced by the specified AD groups. (G and H) Top and Bottom microbial species, respectively. These diagrams detail the number of species that are unique and shared across the three AD groups. Each diagram contains colored regions representing intersections between the groups: red for dementia, green for amyloid, and blue for *APOE ε4*. The numbers within each segment of the diagrams indicate the count of microbial features unique to or shared between the conditions. Specific microbial features are listed in **Table S2**.

Figure 5

Comparison of log-transformed dementia biomarker ratios in CU and AD dementia across two cohorts. (A) The results from the MARS cohort. Box plots show the distribution of log-transformed ratios of top dementia biomarkers to bottom dementia biomarkers for CU individuals (light blue) and AD dementia (dark blue) (Kruskal-Wallis = 31.81, *P* value < .001). (B) The results from a larger validation cohort (n = 448). Box plots present the distribution of log-transformed ratios of top dementia biomarkers to bottom dementia biomarkers found in the MARS cohort for CU individuals (light blue) and people with AD dementia (dark blue) (Kruskal-Wallis = 5.59, *P* value = .02). Each point represents an individual sample, with the boxes indicating the interquartile range (IQR) and the whiskers extending to 1.5 times the IQR. The horizontal line within each box denotes the median value.

Figure 6

Differentially abundant microbial pathways between AD and CU. (A) The distribution of the log ratios of Top/Bottom pathway features between AD (orange) and CU (blue) was shown in a box plot. Mann–Whitney *U* test was performed to determine statistical significance. Asterisks indicate a significant difference between AD (4.90) and CU (2.74) groups in the median of the log ratios of Top/Bottom pathway features (*P* value < .001). (B) A total of 36 differentially abundant features of microbial species and their corresponding pathways between AD and CU were displayed in a forest plot. Circles denote "Top" features, indicating a positive association with AD, whereas triangles denote "Bottom" features, indicating a negative association. The lines are color-coded by unique species and their corresponding pathways. DA analysis was conducted using BIRDMAn. (C) RPCA on the clinical diagnosis group and a biplot of microbiome pathway features and their corresponding species. Each point represents an

individual sample color-coded by the respective group, with CU colored in blue and AD colored in orange. Vectors represent the direction (arrows) and magnitude (length) of the contribution of feature variables to the principal components (PCs). Vectors in red indicate Top features and vectors in green indicate Bottom features. PC1 and PC2 axes represent the most variance in data. Statistical analysis on RPCA was performed with PERMANOVA between AD and CU groups.

Figure 7

Heatmap illustrating the associations between gut microbiome compositional and functional features and CSF biomarkers in AD and related pathologies. (A) This heatmap represents the coefficients of regression analysis between the top and bottom 20 gut microbial species linked to dementia and CSF biomarkers in two groups: Top (more abundant in AD, denoted by the pink bar) and Bottom (less abundant in AD, denoted by the green bar). The color scale indicates the strength and direction of the associations, with red representing positive associations and blue representing negative associations. The intensity of the color corresponds to the magnitude of the coefficient. Listed on the left are the gut microbiome species that were identified as more or less abundant in dementia-AD through BIRDMAn. (B) The heatmap depicts the coefficients of regression analysis between the gut microbial pathways and CSF biomarkers. Coefficients are scaled by colors indicating the strength and direction of the associations, with green representing positive associations and pink representing negative associations. The intensity of the color corresponds to the magnitude (strength) of the coefficient. Microbial species and their associated pathway features are listed on the left of the plot and two groups (Top: more abundant in AD, denoted by the light pink bar; and Bottom: less abundant in AD or more abundant in CU, denoted by the light green bar) from DA analysis using BIRDMAn are displayed on the right of the plot.

The biomarkers listed along the bottom include amyloid pathology ($A\beta_{42}/A\beta_{40}$), tau pathophysiology ($pTau_{181}$ and tTau), neurodegeneration (NfL), synaptic dysfunction and injury (neurogranin and α-synuclein), inflammation (IL-6), and glial activation (S100B, GFAP, YKL-40, and sTREM2). Asterisks indicate the level of statistical significance of the associations: ***P < .001, **P < .01, and *P < .05 (uncorrected).

Table 1. Participant demographics at fecal sample collection by clinical diagnosis.

Variable	N	Overall, N = 232[†]	Dementia-AD, N = 24[†]	CU, N = 208[†]	*P* value[‡]
Age	232	67 (±7)	71 (±7)[§**]	66 (±7)	.002
Sex	232				.7
Female		142 (61%)	16 (67%)	126 (61%)	
Male		90 (39%)	8 (33%)	82 (39%)	
Race	232				>0.9
Black or African American		10 (4.3%)	1 (4.2%)	9 (4.3%)	
White		222 (96%)	23 (96%)	199 (96%)	
***APOE* genotype**	227				<.001
ε2ε3		22 (9.7%)	0 (0%)	22 (11%)	
ε3ε3		120 (53%)	5 (21%)[§**]	115 (57%)	
ε2ε4		5 (2.2%)	0 (0%)	5 (2.5%)	
ε3ε4		64 (28%)	11 (46%)	53 (26%)	
ε4ε4		16 (7.0%)	8 (33%)[§****]	8 (3.9%)	
***APOE ε4* genotype**	227				<.001
Negative (non-carrier)		142 (63%)	5 (21%)	137 (67%)	
Positive (carrier)		85 (37%)	19 (79%)[§****]	66 (33%)	
Bristol stool type	232				.031
1		16 (6.9%)	0 (0%)	16 (7.7%)	
2		19 (8.2%)	3 (13%)	16 (7.7%)	
3		35 (15%)	9 (38%)[§*]	26 (13%)	
4		105 (45%)	6 (25%)	99 (48%)	
5		37 (16%)	4 (17%)	33 (16%)	
6		19 (8.2%)	2 (8.3%)	17 (8.2%)	
7		1 (0.4%)	0 (0%)	1 (0.5%)	
BMI	232	28.2 (±5.4)	26.0 (±4.7)[§*]	28.4 (±5.4)	.030
Amyloid status	145				<.001
0 (A−)		104 (72%)	0 (0%)	104 (78%)	
1 (A+)		41 (28%)	12 (100%)[§****]	29 (22%)	
Medication status	232				.7
medicated		213 (92%)	23 (96%)	190 (91%)	
non-medicated		19 (8.2%)	1 (4.2%)	18 (8.7%)	

Abbreviations: AD, Alzheimer's disease; CU, cognitively unimpaired; *APOE*, apolipoprotein E; BMI, body mass index; A, amyloid status.

NOTE. The Bristol stool types are classification tools for the diagnosis of human feces form.

[†]Mean (±SD); n (%)

[‡]Kruskal-Wallis rank sum test; Pearson's Chi-squared test

[§]Significantly different Dementia-AD vs CU

*P < .05, **P < .01, ***P < .001, ****P < .0001 (P values are Bonferroni test corrected)

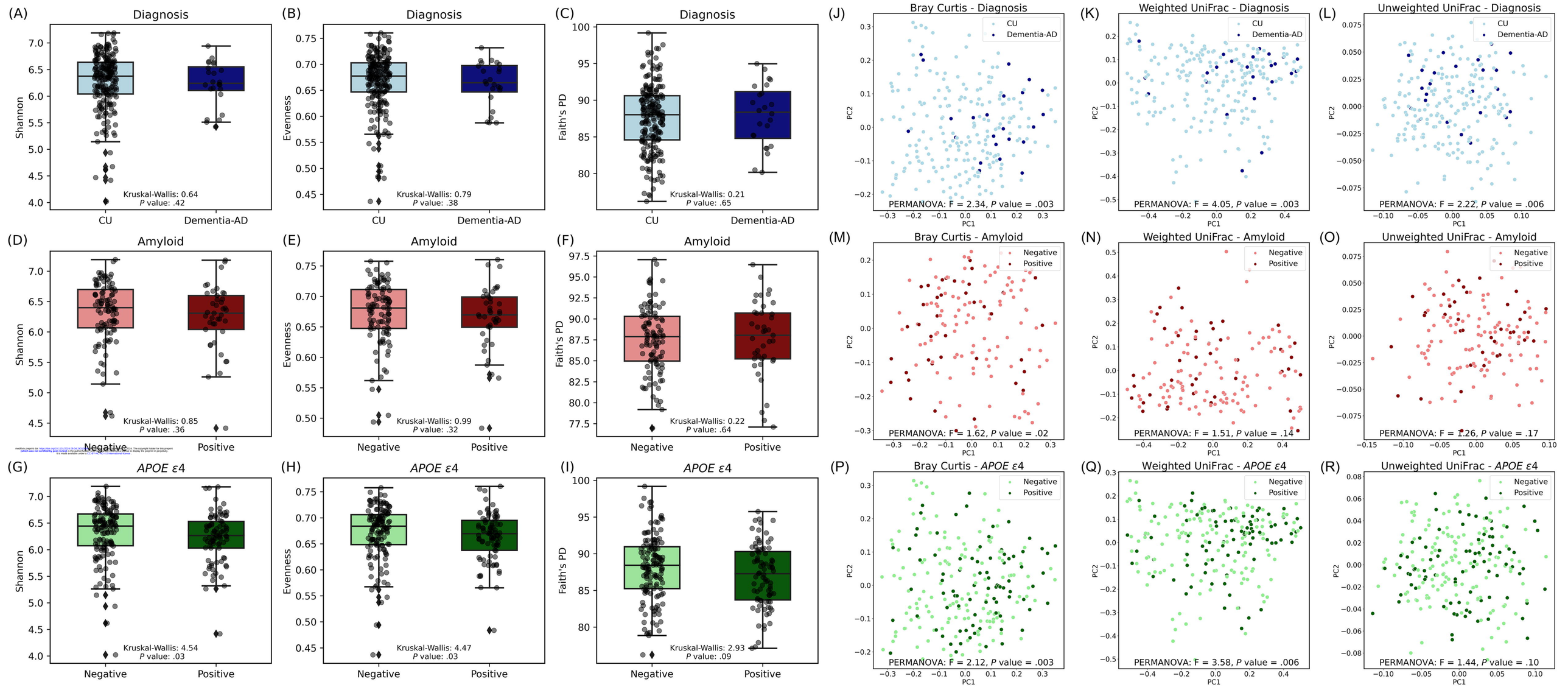
(A)
Diagnosis
Shannon
Kruskal-Wallis: 0.64
P value: .42
CU
Dementia-AD
(B)
Diagnosis
Evenness
Kruskal-Wallis: 0.79
P value: .38
CU
Dementia-AD
(C)
Diagnosis
Faith's PD
Kruskal-Wallis: 0.21
P value: .65
CU
Dementia-AD
(J)
Bray Curtis - Diagnosis
CU
Dementia-AD
PERMANOVA: F = 2.34, P value = .003
PC1
PC2
(K)
Weighted UniFrac - Diagnosis
CU
Dementia-AD
PERMANOVA: F = 4.05, P value = .003
PC1
PC2
(L)
Unweighted UniFrac - Diagnosis
CU
Dementia-AD
PERMANOVA: F = 2.22, P value = .006
PC1
PC2
(D)
Amyloid
Shannon
Kruskal-Wallis: 0.85
P value: .36
Negative
Positive
(E)
Amyloid
Evenness
Kruskal-Wallis: 0.99
P value: .32
Negative
Positive
(F)
Amyloid
Faith's PD
Kruskal-Wallis: 0.22
P value: .64
Negative
Positive
(M)
Bray Curtis - Amyloid
Negative
Positive
PERMANOVA: F = 1.62, P value = .02
PC1
PC2
(N)
Weighted UniFrac - Amyloid
Negative
Positive
PERMANOVA: F = 1.51, P value = .14
PC1
PC2
(O)
Unweighted UniFrac - Amyloid
Negative
Positive
PERMANOVA: F = 1.26, P value = .17
PC1
PC2
(G)
APOE ε4
Shannon
Kruskal-Wallis: 4.54
P value: .03
Negative
Positive
(H)
APOE ε4
Evenness
Kruskal-Wallis: 4.47
P value: .03
Negative
Positive
(I)
APOE ε4
Faith's PD
Kruskal-Wallis: 2.93
P value: .09
Negative
Positive
(P)
Bray Curtis - APOE ε4
Negative
Positive
PERMANOVA: F = 2.12, P value = .003
PC1
PC2
(Q)
Weighted UniFrac - APOE ε4
Negative
Positive
PERMANOVA: F = 3.58, P value = .006
PC1
PC2
(R)
Unweighted UniFrac - APOE ε4
Negative
Positive
PERMANOVA: F = 1.44, P value = .10
PC1
PC2

(A)

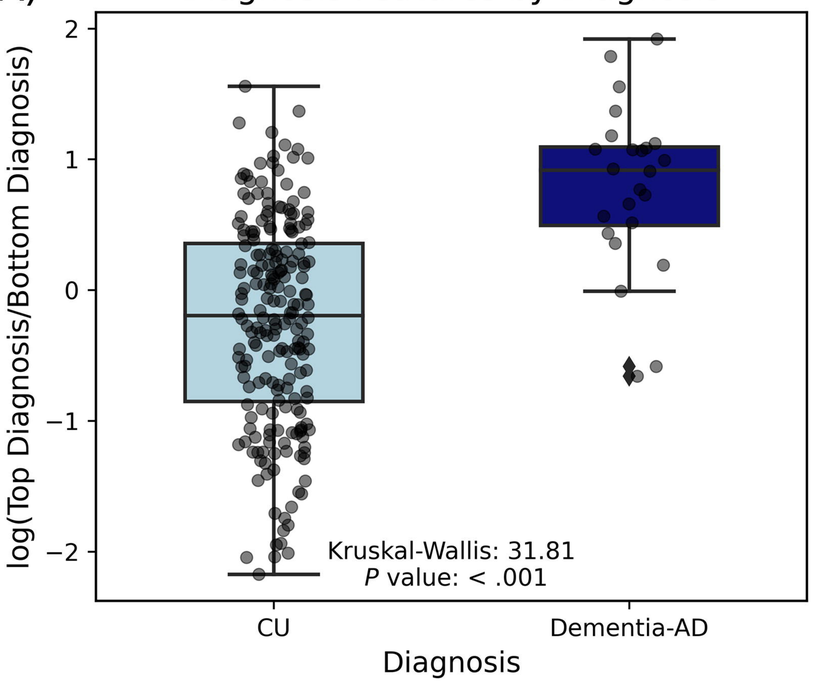
Diagnosis Features by Diagnosis
log(Top Diagnosis/Bottom Diagnosis)
Kruskal-Wallis: 31.81
P value: < .001
CU
Dementia-AD
Diagnosis

(B)

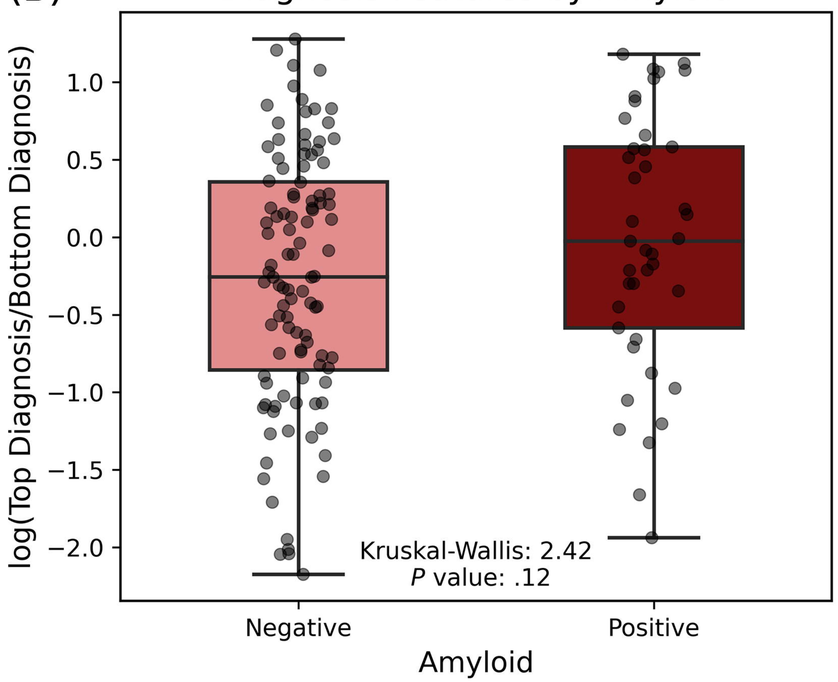
Diagnosis Features by Amyloid
log(Top Diagnosis/Bottom Diagnosis)
Kruskal-Wallis: 2.42
P value: .12
Negative
Positive
Amyloid

(C)

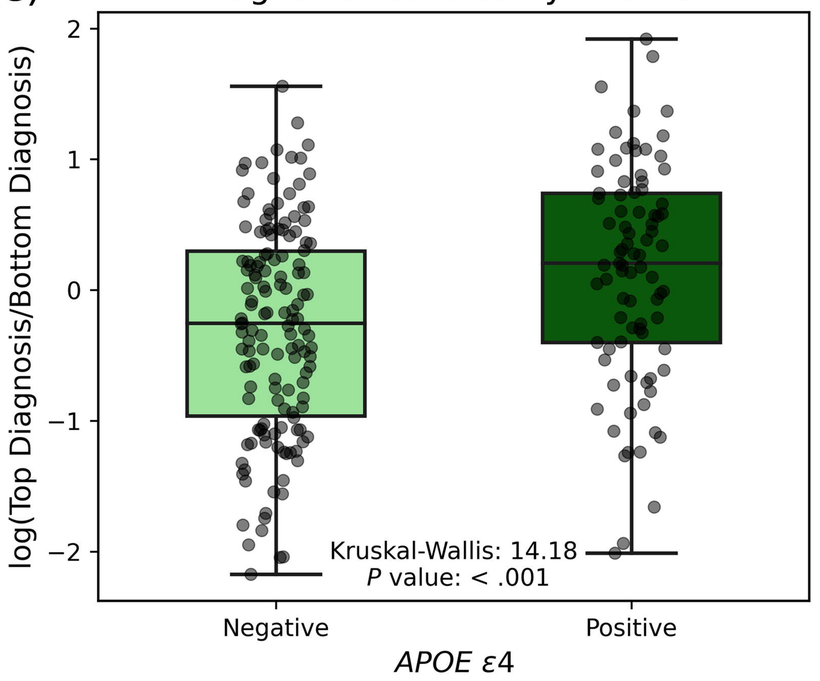
Diagnosis Features by APOE ε4
log(Top Diagnosis/Bottom Diagnosis)
Kruskal-Wallis: 14.18
P value: < .001
Negative
Positive
APOE ε4

(D)

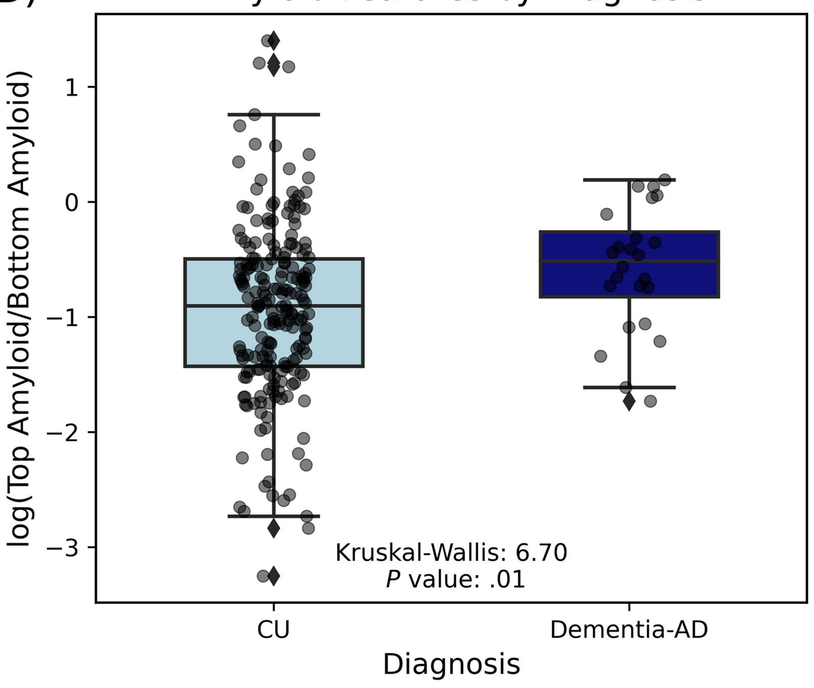
Amyloid Features by Diagnosis
log(Top Amyloid/Bottom Amyloid)
Kruskal-Wallis: 6.70
P value: .01
CU
Dementia-AD
Diagnosis

(E)

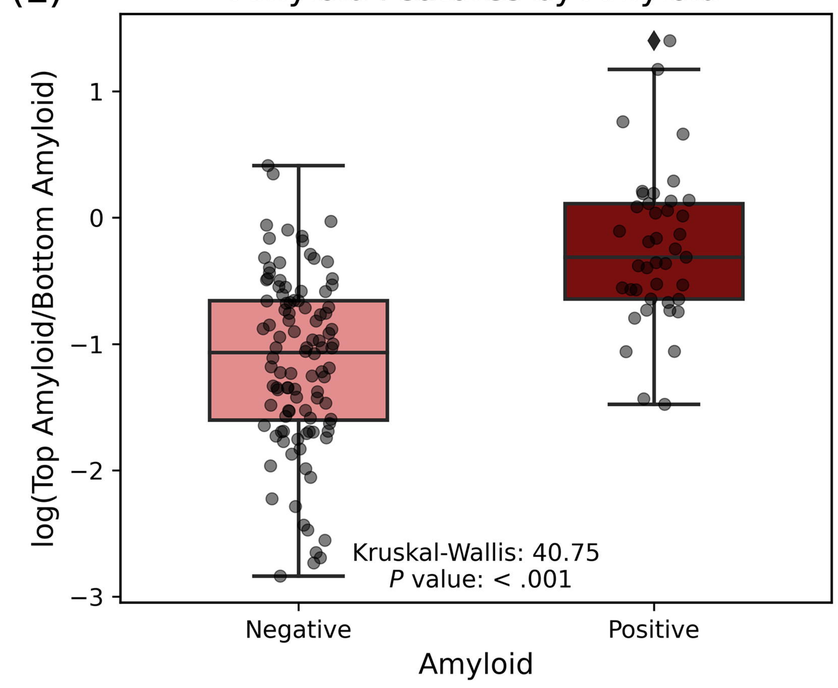
Amyloid Features by Amyloid
log(Top Amyloid/Bottom Amyloid)
Kruskal-Wallis: 40.75
P value: < .001
Negative
Positive
Amyloid

(F)

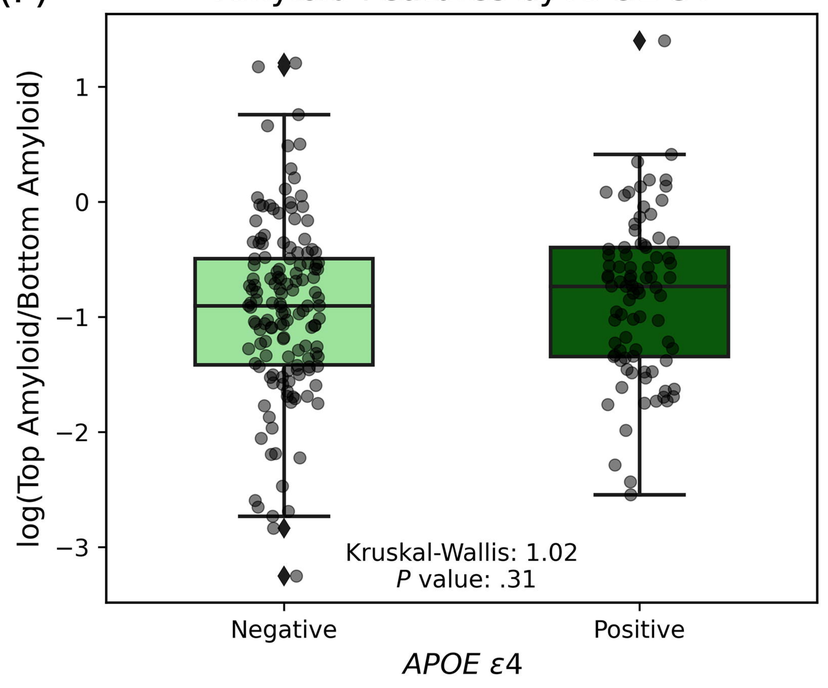
Amyloid Features by APOE ε4
log(Top Amyloid/Bottom Amyloid)
Kruskal-Wallis: 1.02
P value: .31
Negative
Positive
APOE ε4

(G)

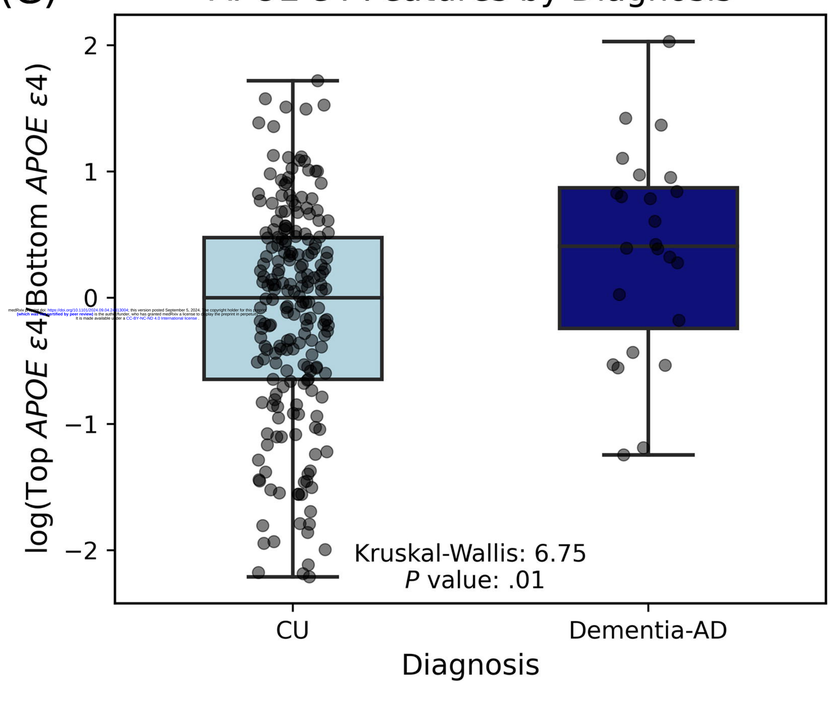
APOE ε4 Features by Diagnosis
log(Top APOE ε4/Bottom APOE ε4)
Kruskal-Wallis: 6.75
P value: .01
CU
Dementia-AD
Diagnosis

(H)

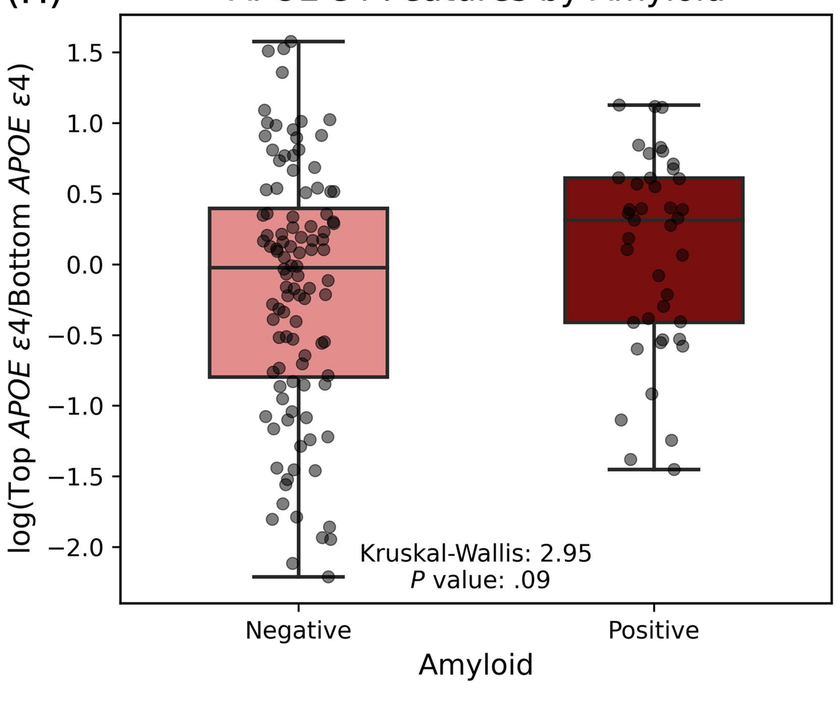
APOE ε4 Features by Amyloid
log(Top APOE ε4/Bottom APOE ε4)
Kruskal-Wallis: 2.95
P value: .09
Negative
Positive
Amyloid

(I)

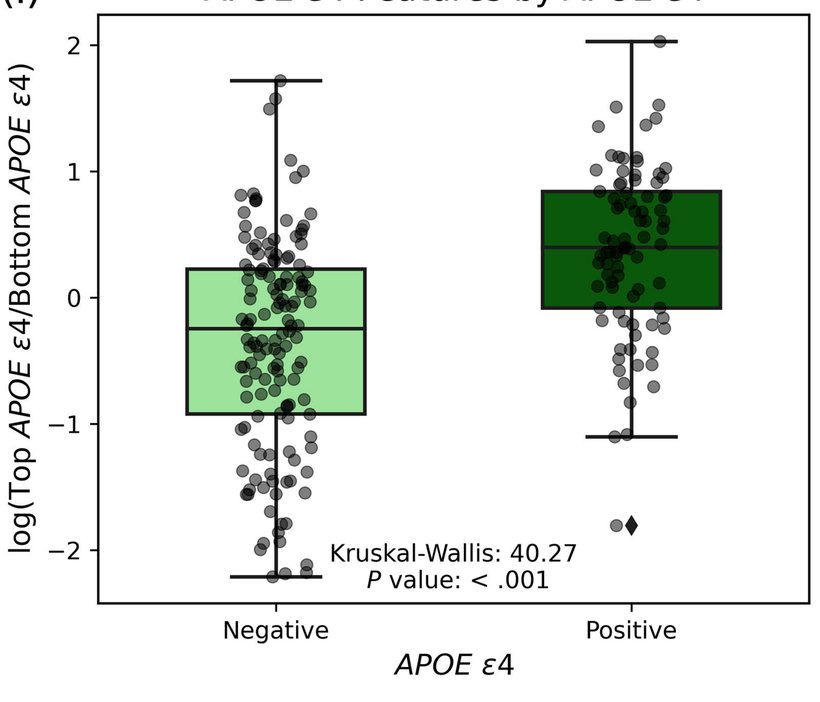
APOE ε4 Features by APOE ε4
log(Top APOE ε4/Bottom APOE ε4)
Kruskal-Wallis: 40.27
P value: < .001
Negative
Positive
APOE ε4

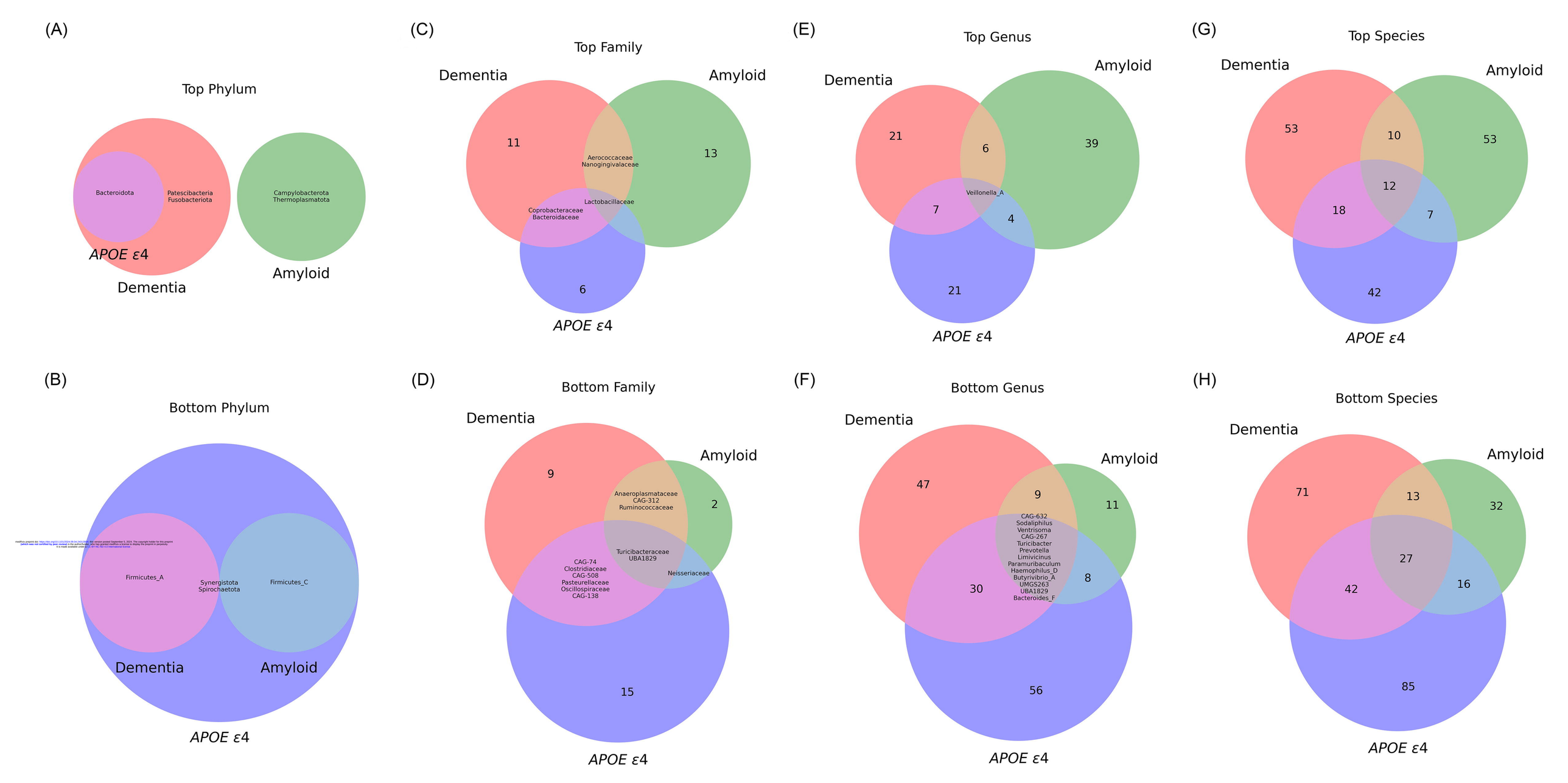

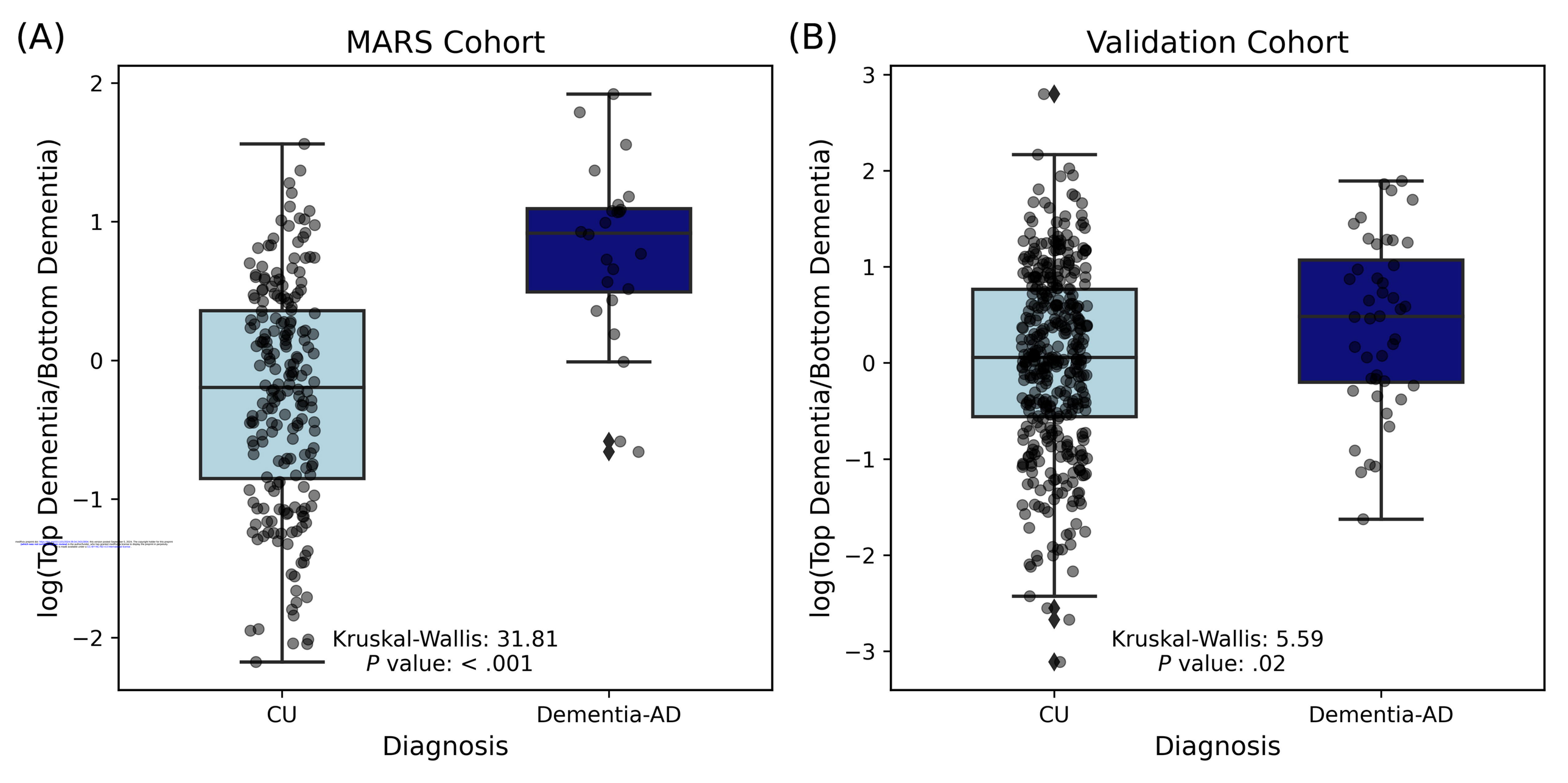
(A)
MARS Cohort
log(Top Dementia/Bottom Dementia)
2
1
0
−1
−2
Kruskal-Wallis: 31.81
P value: < .001
CU
Dementia-AD
Diagnosis
(B)
Validation Cohort
log(Top Dementia/Bottom Dementia)
3
2
1
0
−1
−2
−3
Kruskal-Wallis: 5.59
P value: .02
CU
Dementia-AD
Diagnosis

(A)

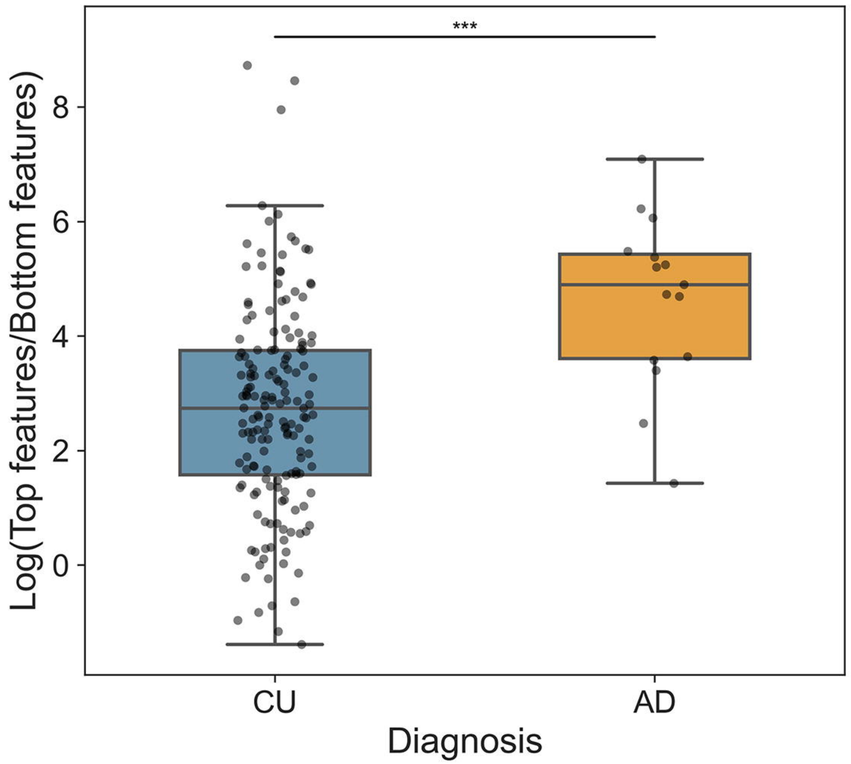
***
Log(Top features/Bottom features)
8
6
4
2
0
CU
AD
Diagnosis

(B)

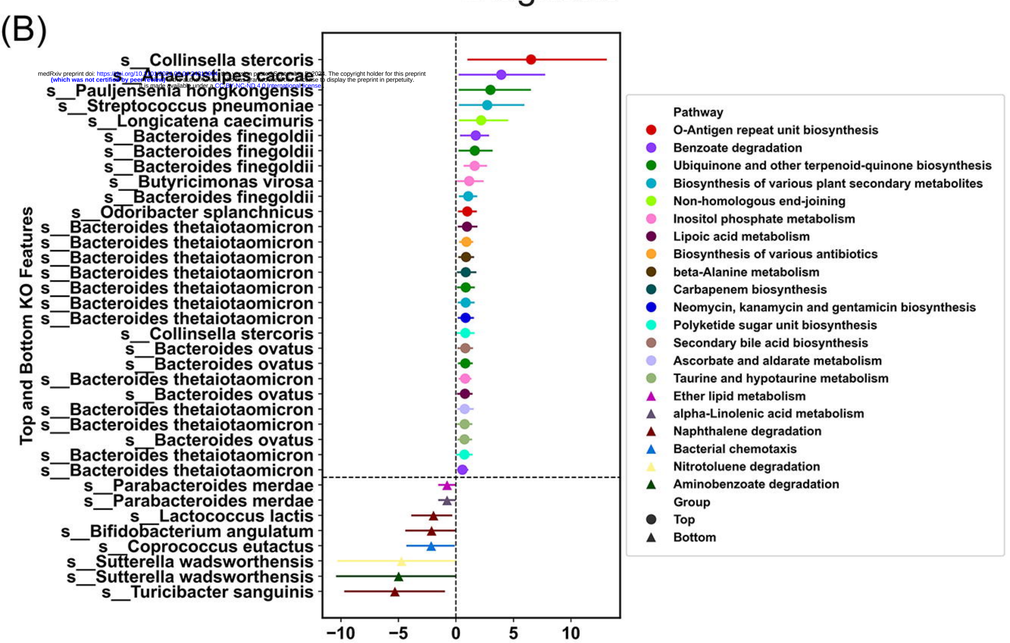
s__Collinsella stercoris
s__Anaerostipes caccae
s__Pauljensenia hongkongensis
s__Streptococcus pneumoniae
s__Longicatena caecimuris
s__Bacteroides finegoldii
s__Bacteroides finegoldii
s__Bacteroides finegoldii
s__Butyricimonas virosa
s__Bacteroides finegoldii
s__Odoribacter splanchnicus
s__Bacteroides thetaiotaomicron
s__Bacteroides thetaiotaomicron
s__Bacteroides thetaiotaomicron
s__Bacteroides thetaiotaomicron
s__Bacteroides thetaiotaomicron
s__Bacteroides thetaiotaomicron
s__Collinsella stercoris
s__Bacteroides ovatus
s__Bacteroides ovatus
s__Bacteroides thetaiotaomicron
s__Bacteroides ovatus
s__Bacteroides thetaiotaomicron
s__Bacteroides thetaiotaomicron
s__Bacteroides ovatus
s__Bacteroides thetaiotaomicron
s__Bacteroides thetaiotaomicron
s__Parabacteroides merdae
s__Parabacteroides merdae
s__Lactococcus lactis
s__Bifidobacterium angulatum
s__Coprococcus eutactus
s__Sutterella wadsworthensis
s__Sutterella wadsworthensis
s__Turicibacter sanguinis
Top and Bottom KO Features
−10
−5
0
5
10
Log Ratio for AD/CU
Pathway
O-Antigen repeat unit biosynthesis
Benzoate degradation
Ubiquinone and other terpenoid-quinone biosynthesis
Biosynthesis of various plant secondary metabolites
Non-homologous end-joining
Inositol phosphate metabolism
Lipoic acid metabolism
Biosynthesis of various antibiotics
beta-Alanine metabolism
Carbapenem biosynthesis
Neomycin, kanamycin and gentamicin biosynthesis
Polyketide sugar unit biosynthesis
Secondary bile acid biosynthesis
Ascorbate and aldarate metabolism
Taurine and hypotaurine metabolism
Ether lipid metabolism
alpha-Linolenic acid metabolism
Naphthalene degradation
Bacterial chemotaxis
Nitrotoluene degradation
Aminobenzoate degradation
Group
Top
Bottom

(C)

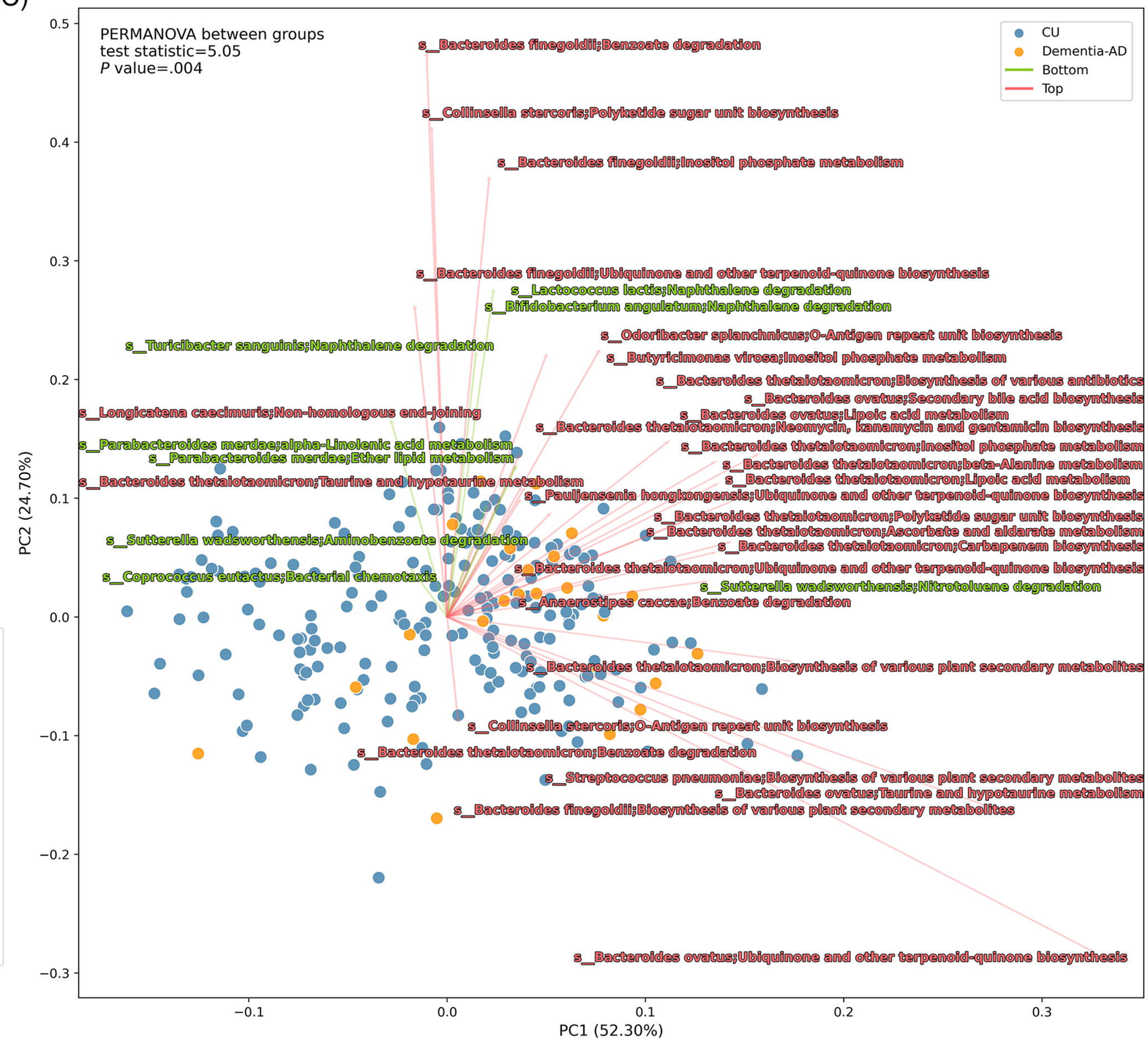
PERMANOVA between groups
test statistic=5.05
P value=.004
CU
Dementia-AD
Bottom
Top
s__Bacteroides finegoldii;Benzoate degradation
s__Collinsella stercoris;Polyketide sugar unit biosynthesis
s__Bacteroides finegoldii;Inositol phosphate metabolism
s__Bacteroides finegoldii;Ubiquinone and other terpenoid-quinone biosynthesis
s__Lactococcus lactis;Naphthalene degradation
s__Bifidobacterium angulatum;Naphthalene degradation
s__Turicibacter sanguinis;Naphthalene degradation
s__Odoribacter splanchnicus;O-Antigen repeat unit biosynthesis
s__Butyricimonas virosa;Inositol phosphate metabolism
s__Bacteroides thetaiotaomicron;Biosynthesis of various antibiotics
s__Bacteroides ovatus;Secondary bile acid biosynthesis
s__Longicatena caecimuris;Non-homologous end-joining
s__Bacteroides ovatus;Lipoic acid metabolism
s__Bacteroides thetaiotaomicron;Neomycin, kanamycin and gentamicin biosynthesis
s__Parabacteroides merdae;alpha-Linolenic acid metabolism
s__Bacteroides thetaiotaomicron;Inositol phosphate metabolism
s__Parabacteroides merdae;Ether lipid metabolism
s__Bacteroides thetaiotaomicron;beta-Alanine metabolism
s__Bacteroides thetaiotaomicron;Taurine and hypotaurine metabolism
s__Bacteroides thetaiotaomicron;Lipoic acid metabolism
s__Pauljensenia hongkongensis;Ubiquinone and other terpenoid-quinone biosynthesis
s__Bacteroides thetaiotaomicron;Polyketide sugar unit biosynthesis
s__Sutterella wadsworthensis;Aminobenzoate degradation
s__Bacteroides thetaiotaomicron;Ascorbate and aldarate metabolism
s__Bacteroides thetaiotaomicron;Carbapenem biosynthesis
s__Coprococcus eutactus;Bacterial chemotaxis
s__Bacteroides thetaiotaomicron;Ubiquinone and other terpenoid-quinone biosynthesis
s__Sutterella wadsworthensis;Nitrotoluene degradation
s__Anaerostipes caccae;Benzoate degradation
s__Bacteroides thetaiotaomicron;Biosynthesis of various plant secondary metabolites
s__Collinsella stercoris;O-Antigen repeat unit biosynthesis
s__Bacteroides thetaiotaomicron;Benzoate degradation
s__Streptococcus pneumoniae;Biosynthesis of various plant secondary metabolites
s__Bacteroides ovatus;Taurine and hypotaurine metabolism
s__Bacteroides finegoldii;Biosynthesis of various plant secondary metabolites
s__Bacteroides ovatus;Ubiquinone and other terpenoid-quinone biosynthesis
PC2 (24.70%)
0.5
0.4
0.3
0.2
0.1
0.0
−0.1
−0.2
−0.3
−0.1
0.0
0.1
0.2
0.3
PC1 (52.30%)

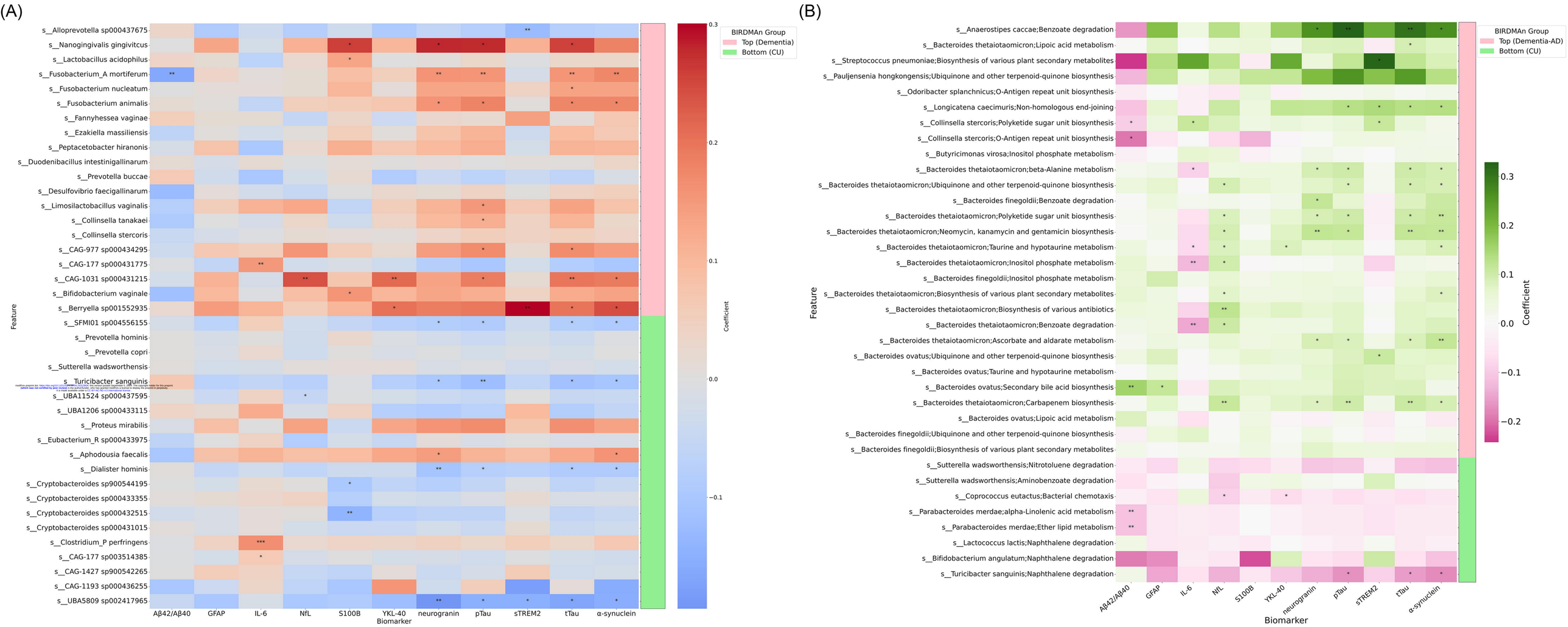
(A)
Feature
s__Alloprevotella sp000437675
s__Nanogingivalis gingivitcus
s__Lactobacillus acidophilus
s__Fusobacterium_A mortiferum
s__Fusobacterium nucleatum
s__Fusobacterium animalis
s__Fannyhessea vaginae
s__Ezakiella massiliensis
s__Peptacetobacter hiranonis
s__Duodenibacillus intestinigallinarum
s__Prevotella buccae
s__Desulfovibrio faecigallinarum
s__Limosilactobacillus vaginalis
s__Collinsella tanakaei
s__Collinsella stercoris
s__CAG-977 sp000434295
s__CAG-177 sp000431775
s__CAG-1031 sp000431215
s__Bifidobacterium vaginale
s__Berryella sp001552935
s__SFMI01 sp004556155
s__Prevotella hominis
s__Prevotella copri
s__Sutterella wadsworthensis
s__Turicibacter sanguinis
s__UBA11524 sp000437595
s__UBA1206 sp000433115
s__Proteus mirabilis
s__Eubacterium_R sp000433975
s__Aphodousia faecalis
s__Dialister hominis
s__Cryptobacteroides sp900544195
s__Cryptobacteroides sp000433355
s__Cryptobacteroides sp000432515
s__Cryptobacteroides sp000431015
s__Clostridium_P perfringens
s__CAG-177 sp003514385
s__CAG-1427 sp900542265
s__CAG-1193 sp000436255
s__UBA5809 sp002417965
Aβ42/Aβ40
GFAP
IL-6
NfL
S100B
YKL-40
neurogranin
pTau
sTREM2
tTau
α-synuclein
Biomarker
BIRDMAn Group
Top (Dementia)
Bottom (CU)
Coefficient
0.3
0.2
0.1
0.0
−0.1
(B)
Feature
s__Anaerostipes caccae;Benzoate degradation
s__Bacteroides thetaiotaomicron;Lipoic acid metabolism
s__Streptococcus pneumoniae;Biosynthesis of various plant secondary metabolites
s__Pauljensenia hongkongensis;Ubiquinone and other terpenoid-quinone biosynthesis
s__Odoribacter splanchnicus;O-Antigen repeat unit biosynthesis
s__Longicatena caecimuris;Non-homologous end-joining
s__Collinsella stercoris;Polyketide sugar unit biosynthesis
s__Collinsella stercoris;O-Antigen repeat unit biosynthesis
s__Butyricimonas virosa;Inositol phosphate metabolism
s__Bacteroides thetaiotaomicron;beta-Alanine metabolism
s__Bacteroides thetaiotaomicron;Ubiquinone and other terpenoid-quinone biosynthesis
s__Bacteroides finegoldii;Benzoate degradation
s__Bacteroides thetaiotaomicron;Polyketide sugar unit biosynthesis
s__Bacteroides thetaiotaomicron;Neomycin, kanamycin and gentamicin biosynthesis
s__Bacteroides thetaiotaomicron;Taurine and hypotaurine metabolism
s__Bacteroides thetaiotaomicron;Inositol phosphate metabolism
s__Bacteroides finegoldii;Inositol phosphate metabolism
s__Bacteroides thetaiotaomicron;Biosynthesis of various plant secondary metabolites
s__Bacteroides thetaiotaomicron;Biosynthesis of various antibiotics
s__Bacteroides thetaiotaomicron;Benzoate degradation
s__Bacteroides thetaiotaomicron;Ascorbate and aldarate metabolism
s__Bacteroides ovatus;Ubiquinone and other terpenoid-quinone biosynthesis
s__Bacteroides ovatus;Taurine and hypotaurine metabolism
s__Bacteroides ovatus;Secondary bile acid biosynthesis
s__Bacteroides thetaiotaomicron;Carbapenem biosynthesis
s__Bacteroides ovatus;Lipoic acid metabolism
s__Bacteroides finegoldii;Ubiquinone and other terpenoid-quinone biosynthesis
s__Bacteroides finegoldii;Biosynthesis of various plant secondary metabolites
s__Sutterella wadsworthensis;Nitrotoluene degradation
s__Sutterella wadsworthensis;Aminobenzoate degradation
s__Coprococcus eutactus;Bacterial chemotaxis
s__Parabacteroides merdae;alpha-Linolenic acid metabolism
s__Parabacteroides merdae;Ether lipid metabolism
s__Lactococcus lactis;Naphthalene degradation
s__Bifidobacterium angulatum;Naphthalene degradation
s__Turicibacter sanguinis;Naphthalene degradation
Aβ42/Aβ40
GFAP
IL-6
NfL
S100B
YKL-40
neurogranin
pTau
sTREM2
tTau
α-synuclein
Biomarker
BIRDMAn Group
Top (Dementia-AD)
Bottom (CU)
Coefficient
0.3
0.2
0.1
0.0
−0.1
−0.2